Productivity and sedimentary δ^{15}N variability for the last 17,000 years along the northern Gulf of Alaska continental slope

Jason A. Addison,[1,2] Bruce P. Finney,[3] Walter E. Dean,[4] Maureen H. Davies,[5] Alan C. Mix,[5] Joseph S. Stoner,[5] and John M. Jaeger[6]

Received 3 May 2011; revised 2 December 2011; accepted 5 December 2011; published 9 February 2012.

[1] Biogenic opal, organic carbon, organic matter stable isotope, and trace metal data from a well-dated, high-resolution jumbo piston core (EW0408–85JC; 59° 33.3′N, 144° 9.21′W, 682 m water depth) recovered from the northern Gulf of Alaska continental slope reveal changes in productivity and nutrient utilization over the last 17,000 years. Maximum values of opal concentration (∼10%) occur during the deglacial Bølling-Allerød (B-A) interval and earliest Holocene (11.2 to 10.8 cal ka BP), moderate values (∼6%) occur during the Younger Dryas (13.0 to 11.2 cal ka BP) and Holocene, and minimum values (∼3.5%) occur during the Late Glacial Interval (LGI). When converted to opal mass accumulation rates, the highest values (∼5000 g cm^{-2} kyr^{-1}) occur during the LGI prior to 16.7 cal ka BP, which points to a strong influence by LGI glacimarine sedimentation regimes. Similar patterns are also observed in total organic carbon and cadmium paleoproductivity proxies. Mid-Holocene peaks in the terrestrial organic matter fraction at 5.5, 4.7, 3.5, and 1.2 cal ka BP indicate periods of enhanced delivery of glaciomarine sediments by the Alaska Coastal Current. The B-A and earliest Holocene intervals are laminated, and enrichments of redox-sensitive elements suggest dysoxic-to-anoxic conditions in the water column. The laminations are also associated with mildly enriched sedimentary δ^{15}N ratios, indicating a link between productivity, nitrogen cycle dynamics, and sedimentary anoxia. After applying a correction for terrestrial δ^{15}N contributions based on end-member mixing models of terrestrial and marine organic matter, the resulting B-A marine δ^{15}N (6.3 ± 0.4 ‰) ratios are consistent with either mild denitrification, or increased nitrate utilization. These findings can be explained by increased micronutrient (Fe) availability during episodes of rapid rising sea level that released iron from the previously subaerial coastal plain; iron input from enhanced terrestrial runoff; and/or the intermittent presence of seasonal sea ice resulting from altered ocean/atmospheric circulation during the B-A in the Gulf of Alaska.

Citation: Addison, J. A., B. P. Finney, W. E. Dean, M. H. Davies, A. C. Mix, J. S. Stoner, and J. M. Jaeger (2012), Productivity and sedimentary δ^{15}N variability for the last 17,000 years along the northern Gulf of Alaska continental slope, *Paleoceanography*, *27*, PA1206, doi:10.1029/2011PA002161.

1. Introduction

[2] The North Pacific Ocean contains the largest high-nutrient-low-chlorophyll (HNLC) region in the Northern Hemisphere (Figure 1a), where primary productivity is limited by iron [*Martin and Fitzwater*, 1988]. In contrast, the coastal regions of both the Northeast and Northwest Pacific are macronutrient-limited (e.g., nitrate and silicic acid [*Whitney et al.*, 2005]). Cross-shelf exchange and vertical mixing of these iron-rich shallow and nitrate-rich deep basinal waters are the chief mechanisms underlying the high seasonal productivity observed in the modern coastal North Pacific (Figure 1b) [*Bruland et al.*, 2001; *Childers et al.*, 2005; *Ladd et al.*, 2005].

[3] Iron availability controls phytoplankton productivity through its influence on the marine N cycle. Nitrogen-fixation by diazotrophic cyanobacteria requires dissolved Fe [*Falkowski et al.*, 1998], and nitrate assimilation by large-celled phytoplankton is inhibited by low ambient-Fe concentrations [*Price et al.*, 1994]. Iron enrichment experiments

[1]Alaska Quaternary Center, University of Alaska Fairbanks, Fairbanks, Alaska, USA.
[2]U.S. Geological Survey, Menlo Park, California, USA.
[3]Department of Geosciences and Department of Biological Sciences, Idaho State University, Pocatello, Idaho, USA.
[4]U.S. Geological Survey, Denver, Colorado, USA.
[5]College of Ocean and Atmospheric Sciences, Oregon State University, Corvallis, Oregon, USA.
[6]Department of Geological Sciences, University of Florida, Gainesville, Florida, USA.

0883-8305/12/2011PA002161

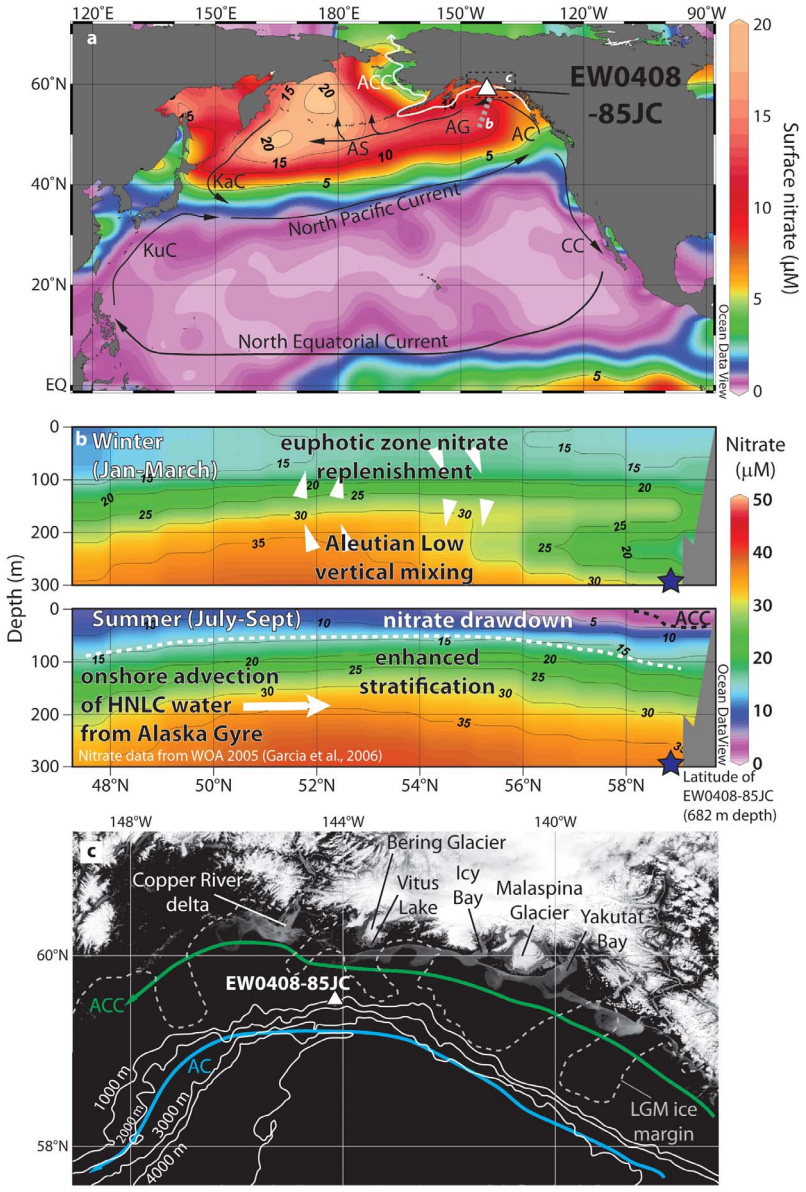

Figure 1. (a) Location of EW0408–85JC (white triangle) and generalized surface circulation of the North Pacific Ocean. Shading and contours indicate annual mean surface nitrate concentrations in μM; data from the 2005 World Ocean Atlas [*Garcia et al.*, 2006] and plotted using Ocean Data View (http://odv.awi.de). Gray dashed line is transect for nitrate sections in Figure 1b. AC = Alaska Current, ACC = Alaska Coastal Current (white line), AG = Alaska Gyre, AS = Alaska Stream, CC = California Current, KaC = Kamchatka Current, KuC = Kuroshio Current. (b) Nitrate concentrations during the winter and summer months along a 300-m-deep transect in the Gulf of Alaska. Note the very low euphotic zone concentrations during the summer following the seasonal primary production bloom. (c) Northern Gulf of Alaska shelf. Solid white lines are 1000-m interval bathymetry contours. Dashed white line indicates Last Glacial Maximum ice margin [*Kaufman and Manley*, 2004]. Base MODIS satellite image taken 22 August 2003 (http://visibleearth.nasa.gov, catalog number 5723). Note extensive light-colored sediment plumes entrained west along shelf by ACC.

in the North Pacific have initiated substantial phytoplankton blooms, particularly among large-celled diatoms, and resulted in significant reductions in nitrate [*Boyd et al.*, 2004; *Coale et al.*, 1996]. Measurements of $\delta^{15}N$ in dissolved and particulate nitrate during the SERIES iron enrichment experiment show progressive enrichment of $^{15}NO_3$ as it was utilized by phytoplankton in the HNLC waters of the Northeast Pacific Ocean [*Needoba et al.*, 2006].

[4] The linkages between iron availability, the N cycle, and marine primary production suggest that a change in

micronutrient input could alter regional productivity through its influence on macronutrient dynamics [*Martin*, 1990]. Building upon this idea, *Davies et al.* [2011] recently suggested inundation of subaerially exposed continental shelves during the Late Glacial Interval (LGI) / Holocene transition could serve as a major source of micronutrients to coastal marine ecosystems. To test this hypothesis, we examine a high-resolution record of paleoproductivity (based on biogenic opal, organic carbon, and cadmium accumulation), $\delta^{15}N$ and $\delta^{13}C$ of bulk organic matter (OM), and trace element concentrations over the last 17 calendar kiloannum before present (cal ka BP) in core EW0408–85JC (59° 33.3′ N, 144° 9.21′W, 682 m water depth) from the continental slope of the northern Gulf of Alaska (Figure 1c).

1.1. Modern Gulf of Alaska Oceanographic Setting

[5] Ocean circulation in the Gulf of Alaska is driven by a dynamic atmosphere-ocean linkage between the Aleutian Low (AL) pressure cell and the Alaska Gyre. Between November to March, the center of the AL is located over the central Gulf of Alaska, resulting in vigorous vertical mixing, reduced sea-surface temperature (SST) and sea level pressure, increased precipitation, and enhanced upwelling in the Alaska Gyre (Figures 1a and 1b) [*Trenberth and Hurrell*, 1994; *Rodionov et al.*, 2005]. During spring and summer, the AL weakens, and the water column becomes stratified by spring snowmelt and radiative warming of the upper water column. Biological productivity in the central gyre is iron-limited, and residual nitrate at the sea surface defines an HNLC area. Cyclonic Alaska Gyre circulation advects shallow nitrate-rich water toward the continental shelf of the Gulf of Alaska where it mixes with iron-rich coastal waters and contributes to large phytoplankton blooms in the spring and summer [*Harrison et al.*, 1999; *Childers et al.*, 2005]. Concurrent with the spring bloom is the seasonal snowmelt pulse along the margin, when freshwater discharge into the Gulf of Alaska is high, and is entrained in the Alaska Coastal Current [*Royer*, 2005].

[6] Iron fluxes to the Gulf of Alaska are derived from a number of sources, including fluvial runoff [*Nishioka et al.*, 2001], suboxic dissolution of iron oxides on the continental shelf [*Chase et al.*, 2007; *Lam and Bishop*, 2008; *Severmann et al.*, 2010], mesoscale eddies [*Johnson et al.*, 2005], and dust storms rich in glacial rock flour [*Crusius et al.*, 2011]. These observations indicate a strong coupling between atmospheric circulation, water column dynamics, and primary productivity [*Gargett*, 1997]. Gulf of Alaska coastal productivity occurs dominantly within a downwelling regime [*Weingartner et al.*, 2002] unlike traditional eastern boundary current settings (e.g., the California Current upwelling system [*Lynn and Simpson*, 1987]). Coastal downwelling is strongest during the winter, and weakens dramatically during the spring and summer with the reduction in wind stress associated with the seasonal relaxation of the AL [*Royer*, 2005].

1.2. Paleoceanographic Setting of the Gulf of Alaska and Other North Pacific Marginal Basins

[7] Relatively few high-resolution records document the paleoceanographic development of the Gulf of Alaska since the Late Glacial Interval (LGI). The complex LGI environment incorporates (1) more than 3,500 km of coastline occupied by the southern Alaska portion of the Cordilleran Ice Sheet [*Kaufman and Manley*, 2004], (2) complex relative and eustatic sea level changes associated with a tectonically active margin [*Gulick et al.*, 2004], and (3) a re-organization of North Pacific Ocean circulation due to the emergence of central Beringia and closure of the Bering Strait during times of low sea level [*Hopkins*, 1959].

[8] Previous work [*Kulm et al.*, 1973; *Molnia*, 1982; *Rea et al.*, 1995; *Rea and Snoeckx*, 1995; *Zahn et al.*, 1991; *de Vernal and Pedersen*, 1997; *McDonald et al.*, 1999; *Galbraith et al.*, 2007, 2008a] suggests that the Gulf of Alaska was cooler, experienced a high ice-rafting sediment flux, and had relatively low primary productivity during the LGI. However, the low sedimentation rates associated with these studies makes detailed inferences about the Gulf of Alaska during the LGI/Holocene transition difficult. Higher-resolution studies from the adjacent Bering Sea and the Sea of Okhotsk suggest these regions had limited productivity during the LGI, and that the eastern Bering Sea was covered in perennial sea ice while the Sea of Okhotsk experienced only seasonal sea ice cover [*Sancetta et al.*, 1984; *Shiga and Koizumi*, 1999; *Seki et al.*, 2004; *Cook et al.*, 2005; *Okazaki et al.*, 2005a, 2005b; *VanLaningham et al.*, 2009; *Caissie et al.*, 2010; *Katsuki et al.*, 2010]. The inundation of the shallow Bering Sea shelf between 12.4 – 11.3 cal ka BP [*Keigwin et al.*, 2006] precedes increases in both siliceous primary productivity and surface salinities in the Bering Sea, as well as a reduction in sea ice cover and terrigenous sediment flux.

[9] The Sea of Okhotsk and the Gulf of Alaska are the modern sources of North Pacific Intermediate Water (NPIW) [*Talley*, 1993; *Wong et al.*, 1998; *You et al.*, 2000]. Several recent studies have suggested the source of NPIW shifted to the Bering Sea during the LGI [*Keigwin*, 2002; *Ohkushi et al.*, 2003; *Horikawa et al.*, 2010]. Changes in NPIW circulation have been linked with paleoenvironmental shifts as distant as the Mexican Pacific margin [*van Geen et al.*, 2003; *Crusius et al.*, 2004].

2. Methods

2.1. Core Description and Chronology

[10] Jumbo piston core EW0408–85JC (59° 33.3′N, 144° 9.21′W, depth 682 m) was recovered by the R/V *Maurice Ewing* from the continental slope along the Gulf of Alaska margin in 2004 (Figure 1c). Following retrieval, the core was cut into 1.5 m sections and analyzed shipboard using a GEOTEK MultiSensor Core Logger (MSCL) to measure high-spatial-resolution seismic velocity, gamma-ray attenuated wet bulk density (WBD), whole-round magnetic susceptibility, and electrical resistivity at 1-cm intervals [*Blum*, 1997]. Each core section was subsequently split, lithologies described and high-resolution linescan imagery was collected. Computerized tomographic (CT) wet bulk density data were also determined [*Davies et al.*, 2011]. All EW0408 sediment cores are archived at the Oregon State University core repository in Corvallis, Oregon. The chronology of EW0408–85JC is based on 37 AMS ^{14}C dates on planktonic foraminifera [*Davies et al.*, 2011] (see Figure S1 in the auxiliary material).[1]

[1]Auxiliary materials are available in the HTML. doi:10.1029/2011PA002161.

2.2. Biogenic Opal

[11] Bulk 1-cm-thick sediment samples of ~10 cm^3 volume were collected from EW0408–85JC at 5 cm intervals. Samples were freeze-dried, homogenized and powdered by hand with a ceramic mortar and pestle, and further subsampled. The first split was treated in 2 N HCl overnight, rinsed with Millipore distilled water three times, and freeze-dried. An aliquot was measured for biogenic silica (opal) using a wet-alkali extraction modified from *Mortlock and Froelich* [1989]. All values are reported as 10% hydrated opal ($SiO_2 \cdot 0.4\ H_2O$) using a multiplier of 2.4 on Si. Estimated uncertainty is 4.6% (calculated as the coefficient of variation), based on replicate measurements of two internal opal-rich sediment standards, which is similar to the results of an interlaboratory comparison for this technique [*Conley*, 1998].

2.3. Organic Matter $\delta^{13}C$, Sedimentary $\delta^{15}N$, Elemental TOC and TN

[12] A carbonate-free subsample was combusted in a Costech 4010 HCNS elemental analyzer to determine total organic carbon (TOC) and total nitrogen (TN) concentrations. The analyzer was coupled to a Finnigan Delta^{plus}XP isotope ratio mass spectrometer for $\delta^{13}C$ and $\delta^{15}N$ measurements. All isotope values are reported in permil units (‰) according to the relationship

$$\delta X = [(R_{sample}/R_{standard}) - 1] \cdot 1000‰, \quad (1)$$

where X is the element of interest and R is the measured isotopic ratio. All carbon isotope measurements are relative to the Vienna Peedee Belemnite (VPDB) standard and all nitrogen measurements are relative to atmospheric nitrogen. Molar ratios of TN:TOC (hereafter referred to as molar N/C ratios) were calculated following *Perdue and Koprivnjak* [2007]. Replicate measurements of internal standards run along with TOC and TN yielded coefficients of variation of 4.4%, 6.9%, respectively, while replicate measurements of internal $\delta^{13}C$ and $\delta^{15}N$ standards yielded 1σ standard deviations of 0.19‰ and 0.20‰, respectively. Isotope measurements were made at the Alaska Stable Isotope Facility at the University of Alaska Fairbanks.

2.4. $CaCO_3$, Lithic Concentrations, and Mass Accumulation Rates

[13] Total inorganic carbon concentrations were measured on untreated bulk sediment samples by coulometry [*Engleman et al.*, 1985] with an estimated error of ±0.1 wt%, and then multiplied by 8.333 (the molar stochiometric ratio of $CaCO_3$/C) to convert to $CaCO_3$ concentrations. Because $CaCO_3$ analysis was performed on a small subset of the larger bulk inorganic geochemical sample set, a linear regression calculated between the coulometric $CaCO_3$ and total Ca concentrations (section 2.5) was used to develop a composite $CaCO_3$ record ($n = 43$, $r = 0.861$, $p < 0.01$) with an estimated error of ±0.6%. The full suite of major biogenic sediment components was then used to estimate the bulk terrigenous content by difference according to the relationship

$$L = 100\% - [\text{opal}\% + CaCO_3\% + (2 \cdot \text{TOC}\%)], \quad (2)$$

where L is the total lithic concentration, 2 · TOC% represents total organic matter (OM) concentration [*Walinsky et al.*, 2009], and the biogenic phases are assumed to fully account for all other components.

[14] The flux rates of the biogenic and lithic phases were determined using mass accumulation rate calculations between AMS ^{14}C dates, such that

$$MAR_{phase} = DBD \cdot SR \cdot \text{phase fraction}, \quad (3a)$$

where MAR_{phase} is the mass accumulation rate of a particular phase, DBD is the dry bulk density, and SR is the sediment accumulation rate in cm ky^{-1} based on the geochronology results of *Davies et al.* [2011]. Each MAR_{phase} was averaged between age control points [*Francois et al.*, 2004]. As the MSCL-measured WBD and the CT-derived density show a highly significant correlation ($n = 1090$, $r = 0.912$, $p < 0.01$), DBD was estimated from the CT density scans, according to the relationship

$$DBD = (1.634 \cdot \text{CT density}) - 1.68. \quad (3b)$$

This equation is a modeled linear regression between wet and dry bulk densities, as these quantities tend to be closely related, and assumes the only controls on DBD is the volume of pore water (a function of bulk density, measured by either CT or MSCL), the density of the pore water (predominantly a function of salinity in marine sediments), and the solid grain density [*Blum*, 1997; *Weber et al.*, 1997]. These quantities were then assigned to be a pore water density of 1.03 g cm^{-3}, a pore water salinity of 32, and a solid grain density of 2.65 g cm^{-3} (e.g., quartz).

2.5. Inorganic Geochemistry

[15] Samples were analyzed for bulk inorganic geochemical composition by a combination of inductively coupled plasma optical emission spectrometry (ICP-OES) and ICP mass spectrometry (ICP-MS) at SGS Minerals Services in Toronto, Canada. Samples were digested in a sequential acid leaching method using HNO_3, HCl, HF, and $HClO_4$. Samples were then divided into 2 aliquots for analysis by ICP-OES and ICP-MS that yielded a suite of 40 element concentrations. A combination of replicate samples, USGS standards (SGR-1 and PBD-1), and an international standard (NBS-SRM1646) were analyzed within the analytical runs to monitor accuracy and precision. The mean percentage difference between analyzed concentrations and literature values for the standards for all elements was 11%, and most elements are within the reported 1σ range. A mean coefficient of variation for all elements calculated from all replicate samples was 4.1%.

[16] Water column paleoanoxia conditions were inferred from a suite of redox-sensitive trace elements. Whereas several of these elements (S, Mo, U, and Cd) were discussed by *Barron et al.* [2009], the coupling between redox biogeochemical cycling and the independent productivity data sets of opal and TOC are of primary interest in this paper [*Morel and Price*, 2003]. Redox-sensitive elements are predominantly derived from three sources: (1) a lithogenic source associated with terrestrially derived detrital mineral phases; (2) a biogenic source from organic particles via substitution or adsorption processes; (3) a hydrogenous source from precipitation and adsorption reactions from seawater as reduced sulfide phases sensitive to prevailing Eh conditions within the water column or sediment pore waters [*Calvert and Pedersen*, 1993; *Tribovillard et al.*, 2006; *Piper and Calvert*, 2009]. To estimate these different contributions,

the excess fraction was calculated based on normalization of the detrital fraction to a global average sediment composition, assuming a constant aluminosilicate-hosted terrigenous detrital composition where

$$excess\,M = M_{\text{measured}} - [Al_{\text{measured}} \cdot (M/Al)_{\text{avg sed}}], \quad (4)$$

where M_{measured} is the measured concentration of the metal of interest M, and $(M/Al)_{\text{avg sed}}$ is the global mean sediment Al-normalized ratio for metal M [*McLennan*, 1995; *Van der Weijden*, 2002].

2.6. Statistical Analysis

[17] Bivariate Pearson correlation coefficients were calculated for natural-log-transformed data sets to ensure normal distributions [*Davis*, 2002]. Natural-log transformation of percentages has the added benefit of circumventing the constant-sum problem [*Aitchison*, 1986, 1999]. For correlation calculations, all concentration data were ln-transformed prior to analysis.

3. Results

3.1. Core Lithology and Geochronology

[18] An analysis of sediment lithology, stratigraphy, and geochronology for core EW0408–85JC is presented by *Davies et al.* [2011] (Figure S1). The age-depth model indicates that this core contains a continuous record spanning the last 17.3 cal ka BP. The lowermost lithologic unit is a massive dark gray diamict that extends from 831 cm below the seafloor (cmbsf) to the bottom of the core at 1278 cmbsf, and represents rapid ice-proximal sedimentation (613 ± 409 cm ka^{-1}) in the latter part of the LGI. This diamict is overlain by a low-density laminated hemipelagic sediment unit that occurs between 797 and 831 cmbsf (29 ± 19 cm ka^{-1}) that spans the Bølling-Allerød (B-A) warm period identified in the North Atlantic [*Rasmussen et al.*, 2006] and the time of sea level rise associated with Meltwater Pulse (MWP) 1a in Barbados coral records [*Fairbanks*, 1989; *Bard et al.*, 1990; *Deschamps et al.*, 2009], with an abrupt onset at 14.69 ± 0.85 cal ka BP. Between 760 and 797 cmbsf, EW0408–85JC is composed of a moderately high-density, bioturbated sediment that accumulated at a mean rate of 19 ± 11 cm ka^{-1}, best characterized as a sandy silt containing dispersed coarse sand as ice-rafted debris with a basal age of 12.99 ± 0.19 cal ka BP, coeval with the onset of the Younger Dryas in Greenland [*Rasmussen et al.*, 2006]. The uppermost portion of EW0408–85JC is a hemipelagic mud that extends to 760 cmbsf (or 11.16 ± 0.13 cal ka BP) that accumulated at a mean rate of 65 ± 29 cm ka^{-1}. Although the majority of this upper unit is a massive bioturbated dark gray silty clay, the bottom 15 cm is characterized by a weakly laminated interval of lower-density sediment that was deposited during the early Holocene between 11.14 ± 0.09 and 10.75 ± 0.22 cal ka BP. This interval has been linked to a period of rapid eustatic sea level rise known as MWP-1b [*Fairbanks*, 1989; *Bard et al.*, 1990].

3.2. Paleoproductivity Proxies

[19] Biogenic sediment concentrations suggest a high degree of variability in Gulf of Alaska marine productivity since the LGI. Both opal and TOC have higher concentrations in sediments deposited during the B-A and MWP-1b intervals than in sediments deposited during the LGI and YD (Figure 2). Natural-log-transformed opal and TOC concentrations are significantly correlated ($n = 165$, $r = 0.718$, $p < 0.01$), suggesting a preservational bias has not decoupled the accumulation of these biogenic phases given the different conditions under which these components are preserved [*Hedges et al.*, 1999; *Ragueneau et al.*, 2000]. $CaCO_3$ concentrations are low and do not correspond with the concentrations of other biogenic components, as $CaCO_3$ values tend to be high during both the LGI and YD intervals (Figure 2). The lithic concentrations (Figure 2) are highest during the LGI (mean 92.8%), intermediate during the Holocene (89.7%), and lowest during the B-A and MWP-1b intervals (85.0% and 86.6%, respectively). Lithic concentrations are negatively correlated with opal, TOC, and $CaCO_3$, and positively correlated with CT density (all exceed the 99% confidence level).

[20] Cadmium concentrations are positively correlated with opal ($n = 110$, $r = 0.416$, $p < 0.01$), whereas excess Cd is only present during the B-A and MWP-1b intervals (Figure 2). Unlike most trace elements that are redox-sensitive, Cd accumulation is more sensitive to the biogenic flux than ambient dissolved oxygen concentrations due to its micronutrient status [*Lee et al.*, 1995; *Lane and Morel*, 2000; *Lane et al.*, 2005]. Cadmium mass balance calculations in Cariaco Basin sediments partitioned between the water column and detrital, biogenic, and authigenic sediment phases also indicate that Cd is dominantly of biogenic origin (86%) [*Piper and Dean*, 2002]. Elevated concentrations of Cd are found in TOC- and Mo-rich sediments in the Santa Barbara Basin [*Ivanochko and Pedersen*, 2004], the Santa Lucia continental slope [*Hendy and Pedersen*, 2005] and on the Pacific margin of southern Baja [*Dean et al.*, 2006], as well as in laminated Holocene sediments along the Mexican Pacific margin, where concentrations of Cd in non-lithogenic settling particles are similar to those of planktonic values [*Nameroff et al.*, 2002]. Authigenic Cd precipitation (probably as CdS) can occur under anoxic conditions [*Rosenthal et al.*, 1995], though the rate of precipitation may not necessarily be controlled by dissolved sulfide concentrations [*Sundby et al.*, 2004]. Based on these collective observations, it seems most appropriate to consider Cd as a semiquantitative indicator of enhanced biogenic sedimentation, rather than an indicator of water column and/or sediment pore water anoxia. When paired with the other measures of productivity in EW0408–85JC, these diverse multiproxy data (e.g., opal, TOC, and Cd) are consistently high during the B-A and MWP-1b intervals, moderate during the Holocene and YD, and low during the LGI.

3.3. Organic Matter $\delta^{13}C$, Sedimentary $\delta^{15}N$, and Molar N/C Ratios

[21] The sedimentary $\delta^{13}C$, $\delta^{15}N$, and molar N/C ratios vary between −26.3 to −22.1‰, 2.2 to 6.7‰, and 0.04 to 0.11, respectively (Figures 3 and 4). These elemental and isotopic ranges reflect mixing marine and terrestrial organic matter (OM), as well as potential variability in the isotopic composition of marine-derived OM. The LGI samples are similar to sediments derived from modern Bering Glacier outwash, whereas the Holocene sediments in EW0408–85JC are analogous to the surface-sediment OM compositions

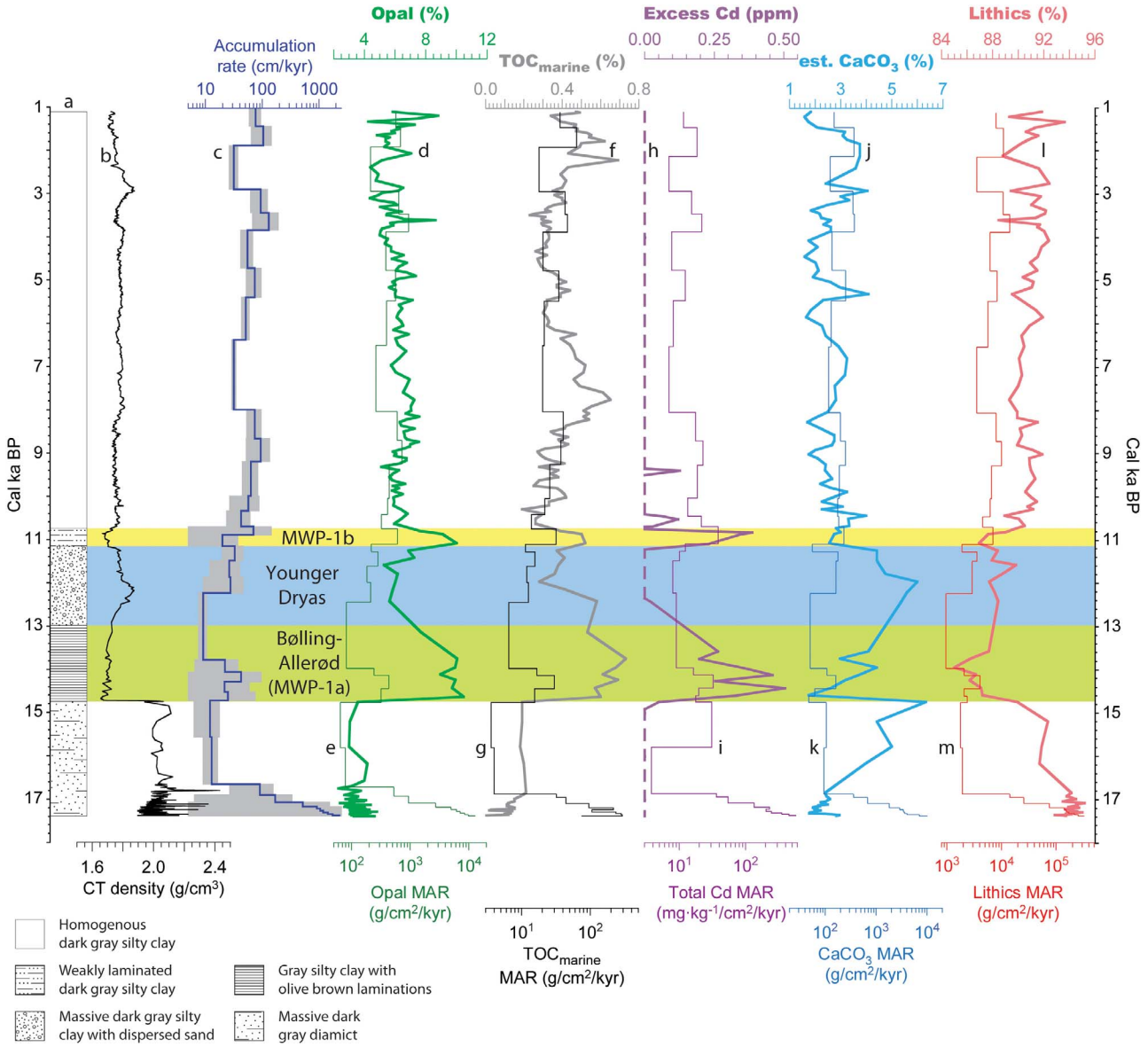

Figure 2. Concentrations (thick lines) and mass accumulation rates (thin lines) for biogenic and lithic components in EW0408–85JC: (a) simplified lithology; (b) CT-derived wet bulk density; (c) sedimentation rate plotted with 1-σ error envelope; (d, e) opal; (f, g) TOC_{marine}; (h, i) Cd; (j, k) $CaCO_3$; and (l, m) lithic fractions. Note all MAR values are plotted on a log axis, and that dashed lines indicate excess Cd concentrations <0 ppm.

measured for offshore locations along the modern northern Gulf of Alaska shelf (Figure 3) [*Walinsky et al.*, 2009].

[22] To estimate the relative proportions of marine and terrestrial OM, a linear mixing model (Table 1) was employed following the results of *Walinsky et al.* [2009] on surface-sediment samples along the Gulf of Alaska margin. Three end-members are marine phytoplankton, vascular plant detritus, and soil OM [*Meyers*, 1994; *McQuoid et al.*, 2001; *Geider and La Roche*, 2002; *Gaye-Haake et al.*, 2005; *Walsh et al.*, 2008]. Here, soil OM was negligible (Figure 3). Using $\delta^{13}C_{terr}$ and $\delta^{13}C_{marine}$ end-member compositions of −26 and −21‰, respectively, yields mean terrestrial OM contributions (m_{terr}) of approximately 0.50, 0.46, 0.37, 0.43, and 0.77 for Holocene, MWP-1b, YD, B-A, and LGI intervals, respectively (Figure 4). A formulation of

$$m_{terr} = [A_{sample} - A_{marine}]/[A_{terr} - A_{marine}] \quad (5)$$

using molar N/C values of 0.025 and 0.125 for the terrestrial and marine end-members yield similar results (Figure 4) (see Table 1 for more information on equations (5), (6), and (7)). The downcore plot of marine organic matter-derived TOC (TOC_{marine}), calculated using

$$TOC_{marine} = TOC_{sample} - (m_{terr} \times TOC_{sample}) \quad (6)$$

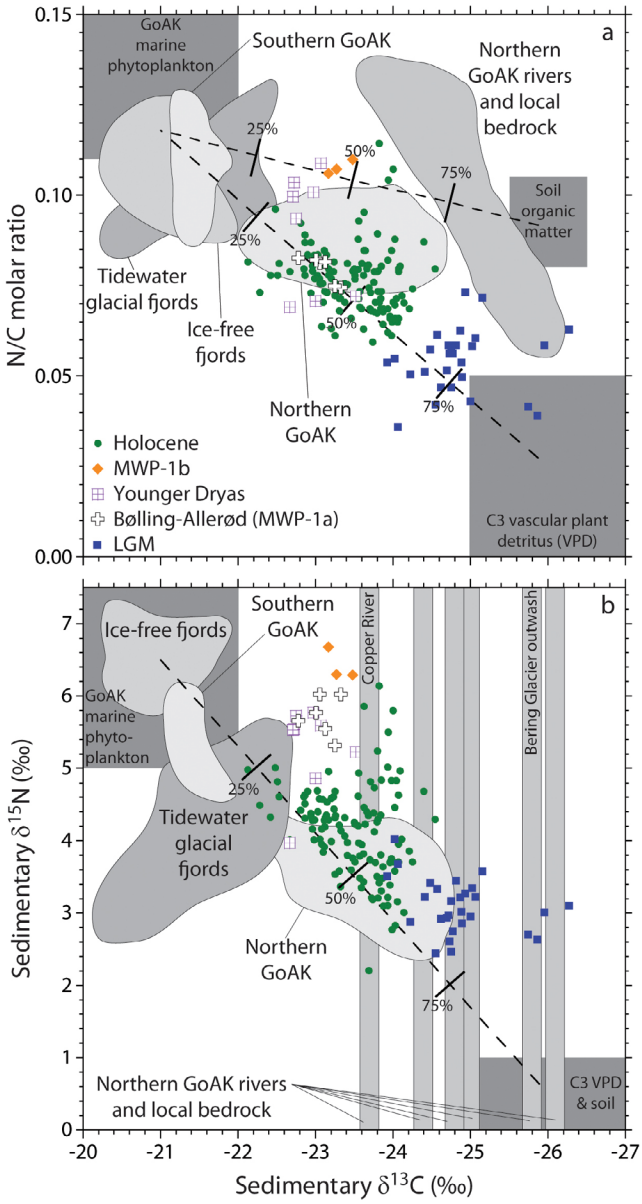

Figure 3. EW0408–85JC organic matter (OM) provenance diagrams utilizing carbonate-free sedimentary $\delta^{13}C$ compared against (a) molar N/C and (b) sedimentary $\delta^{15}N$ ratios. Lightly shaded regions are based on coastal Gulf of Alaska surface sediment data [*Walinsky et al.*, 2009], with north and south defined relative to 58°N latitude. No $\delta^{15}N$ data were reported for fluvial or bedrock samples. Dashed lines represent linear mixing models between potential OM sources; values indicate proportion of total terrestrial (plant and/or soil OM) contribution. GoAK = Gulf of Alaska, VPD = vascular plant detritus.

is similar to those of total TOC and opal (Figure 4), with maxima in the B-A and MWP-1b intervals.

[23] A comparison of the downcore trends in molar N/C ratio, sedimentary $\delta^{13}C$, and $\delta^{15}N$ data show several coherent patterns (Figure 4). LGI sediments are composed of relatively low molar N/C ratios, and depleted $\delta^{13}C$ and $\delta^{15}N$ values. These characteristics, along with the low opal concentrations (<4.8%) are consistent with predominantly terrestrial-derived OM and low export productivity. This contrasts with the opal maxima seen during the B-A and MWP-1b intervals, both of which are associated with moderate N/C ratios (0.07 to 0.08) and higher $\delta^{13}C$ and $\delta^{15}N$ (mean values of −23.2‰ and 5.9‰, respectively). The YD interval has opal values similar to Holocene concentrations (mean 6.1%), a lower mean N/C ratio of 0.09, a mean sedimentary $\delta^{13}C$ value of −22.8‰, and a mean $\delta^{15}N$ value of 5.3‰. Holocene sediments have moderate opal concentrations (mean 8.8%) with little variability, but in-phase shifts in the molar N/C ratio, and sedimentary $\delta^{13}C$ and $\delta^{15}N$ occur during the mid- and late Holocene intervals (after 7 cal ka BP).

3.4. Mass Accumulation Rates

[24] When the biogenic and lithic concentrations are included in mass accumulation rate calculations (equation (3a)), these proxies all show a coherent pattern of enhanced accumulation at the base of EW0408–85JC during the LGI prior to 16.7 cal ka BP, reduced accumulation during the LGI termination (16.7 to 15 cal ka BP), latest part of the B-A, and early part of the YD, and heightened peaks within the B-A and MWP-1b intervals (Figure 2). The correspondence between the biogenic fluxes, the lithic MAR, and sediment accumulation rate trends suggest that MAR calculations are mainly controlled by sedimentation rate, and are not truly representative of export productivity, especially during the LGI. Higher opal, TOC, and Cd fluxes during the B-A and MWP-1b intervals are congruent with measured maximum concentrations of these biogenic phases during these same periods, indicating that these deglacial periods were more productive.

3.5. Redox-Sensitive Elements

[25] Many trace elements are sensitive to reducing or oxidizing conditions in the water column, but we focus on Mn, U, and Mo because these elements are the most sensitive to oxic (Mn) and anoxic/sulfidic (U and Mo) conditions [*Calvert and Pedersen*, 1993; *Tribovillard et al.*, 2006; *Piper and Calvert*, 2009]. Concentrations of Co and Cr track the oxic/suboxic boundary [*Tribovillard et al.*, 2006]. High excess concentrations of Mo and U are indicative of bottom water anoxia during deposition of laminated B-A and early Holocene intervals (Figure 5), which are also contemporaneous with high TOC and opal concentrations (Figure 2). High excess Mn and Co, and minimal excess Mo, U, and Cr within the YD interval imply either suboxic or oxygenated bottom waters. The loss of all excess U and Mo during the Holocene, and the monotonic increase in excess Mn and Co concentrations, suggest increasingly oxic water conditions. Excess Cr is also highest in Holocene sediments, which may indicate some suboxia.

4. Discussion

4.1. Relationships Between Productivity and Environmental Proxies

4.1.1. The Late Glacial Interval in the Gulf of Alaska

[26] The biogenic sediment preserved in EW0408–85JC presents the first high-resolution productivity record spanning the LGI to late Holocene for the northeastern Gulf of Alaska continental slope. This unique location captures primary productivity changes, but also is influenced by Cordilleran Ice Sheet dynamics during the LGI and subsequent deglaciation. For example, the order-of-magnitude

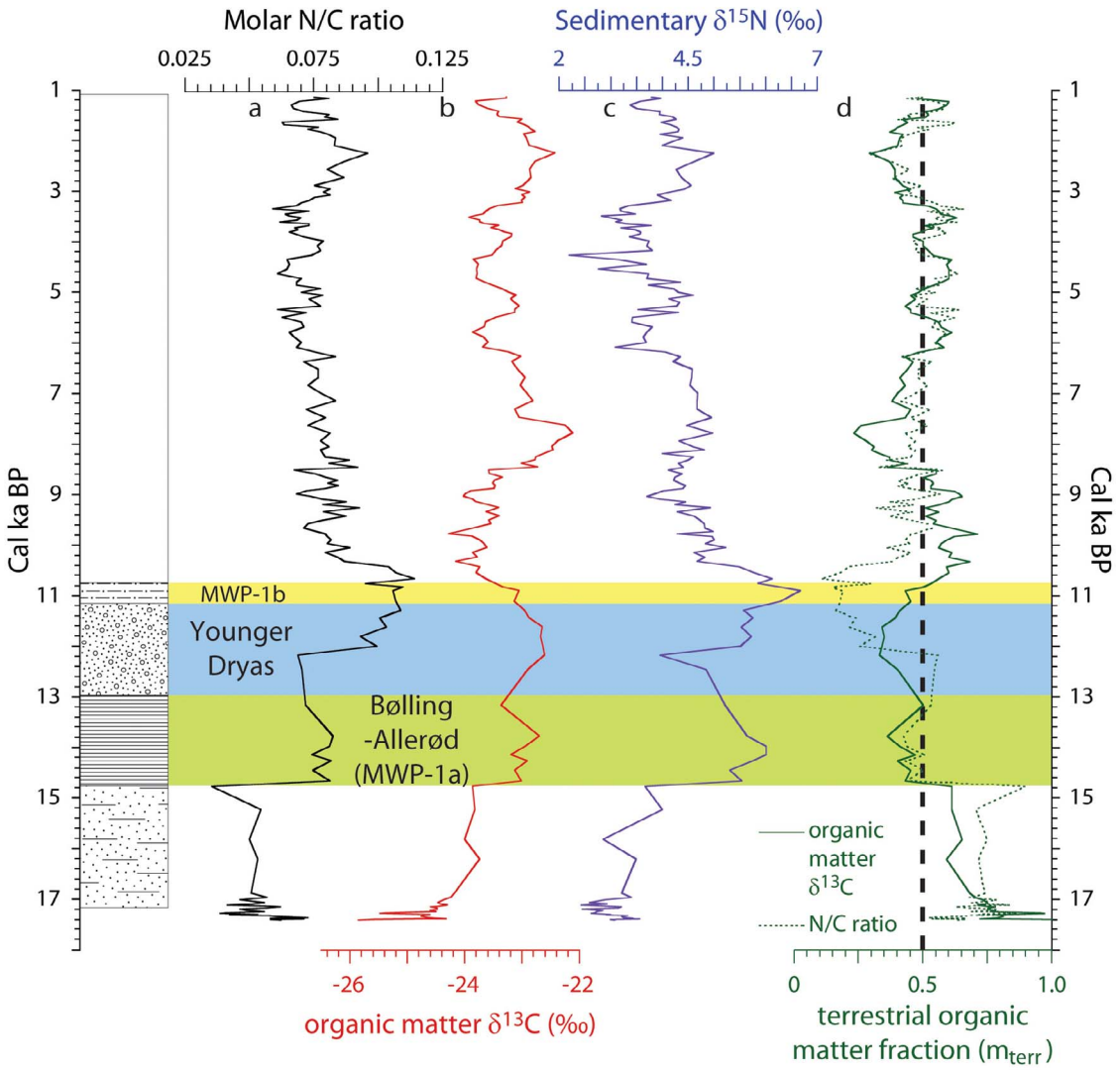

Figure 4. Carbonate-free bulk OM (a) molar N/C ratio, (b) $\delta^{13}C$, and (c) $\delta^{15}N$ results from EW0408–85JC. (d) The contribution of terrestrial-derived OM (mterr) was calculated using equation (5) with mean terrestrial and marine end-member compositions from both $\delta^{13}C$ and N/C ratio data sets. Thick black dashed line indicates 50% terrestrially derived OM contribution. Lithology patterns same as Figure 2.

difference in sedimentation rates between the Holocene and older LGI intervals (17 to 15 cal ka BP) results in mean opal MARs of 511 g cm^{-2} ky^{-1} and 5369 g cm^{-2} ky^{-1}, respectively (Figure 2). The higher values in older LGI sediments seem unlikely to reflect higher productivity within the LGI Gulf of Alaska, and probably instead reflect higher burial efficiency or sediment focusing under higher sedimentation rate conditions. The LGI sediments contain low concentrations of autochthonous marine OM, as evidenced by low opal, TOC_{marine}, and excess Cd concentrations (Figure 2), but contain high concentrations of terrestrially derived OM ($m_{terr} > 0.7$; Figure 4). Given the lack of terrestrial vegetation present along the Gulf of Alaska margin during this cold period [*Peteet and Mann*, 1994], it seems likely that the high concentrations of allochthonous OM are derived primarily from eroding sedimentary bedrock [*Walinsky et al.*, 2009].

[27] These observations imply the LGI Gulf of Alaska continental slope was functionally similar to one of the many glaciated fjords along the modern coast, with a cold, fresh, and strongly stratified euphotic zone [*de Vernal and Pedersen*, 1997], high concentrations of suspended sediment, extremely low primary productivity, icebergs, and seasonal sea ice [*Barron et al.*, 2009]. Sedimentation rates associated with the older LGI section, though consistent with glacial delivery, are too low to represent a full proximal glaciomarine sedimentation regime [*Powell and Molnia*, 1989; *Jaeger et al.*, 1998].

4.1.2. The LGI/Holocene Transition

[28] The regional Cordilleran Ice Sheet likely retreated from the ocean onto land around 14.8 cal ka BP [*Davies et al.*, 2011]. The majority of sea-ice and sea-ice-related diatom taxa and subarctic silicoflagellate taxa disappear from EW0408–85JC at the end of the Younger Dryas around 11.7 cal ka BP [*Barron et al.*, 2009], and dinocyst-based transfer functions from a nearby site indicate the onset of modern regional surface salinities (>32) by at least 10.2 cal ka BP [*de Vernal and Pedersen*, 1997]. The onset of full

Table 1. Terms and Values Used for Calculating m_{terr}, TOC_{marine}, and $\delta^{15}N_{marine}$[a]

Term	Maximum Range	Minimum Range	Mean Range
	(i) End-Member Compositions for Equations (5) and (7), Using Organic Matter $\delta^{13}C$		
$\delta^{13}C_{terr}$	−27 ‰	−25 ‰	−26 ‰
$\delta^{13}C_{marine}$	−20 ‰	−22 ‰	−21 ‰
$\delta^{15}N_{terr}$	0 ‰	1 ‰	0.5 ‰
	(ii) End-Member Compositions for Equations (5) and (7), Using Molar N/C Ratios		
$(N/C)_{terr}$	0.00	0.05	0.025
$(N/C)_{marine}$	0.15	0.10	0.125
$\delta^{15}N_{terr}$	0 ‰	1 ‰	0.5 ‰
	(iii) Measured Values for Equations (5), (6), and (7)		
$\delta^{13}C_{sample}$	as measured by isotope-ratio mass spectrometer		
$\delta^{15}N_{sample}$	as measured by isotope-ratio mass spectrometer		
TOC_{sample}	as measured by HCNS elemental analyzer		
$(N/C)_{sample}$	as measured by HCNS elemental analyzer		

[a]Equation (5): $m_{terr} = [A_{sample} - A_{marine}] / [A_{terr} - A_{marine}]$, where A refers to the end-member compositions in (i) or (ii) and the corresponding measured value in (iii). Equation (6): $TOC_{marine} = TOC_{sample} - (m_{terr} \times TOC_{sample})$. Equation (7): $\delta^{15}N_{marine} = [\delta^{15}N_{sample} - (m_{terr} \times \delta^{15}N_{terr})] / m_{marine}$, where $m_{marine} = 1 - m_{terr}$.

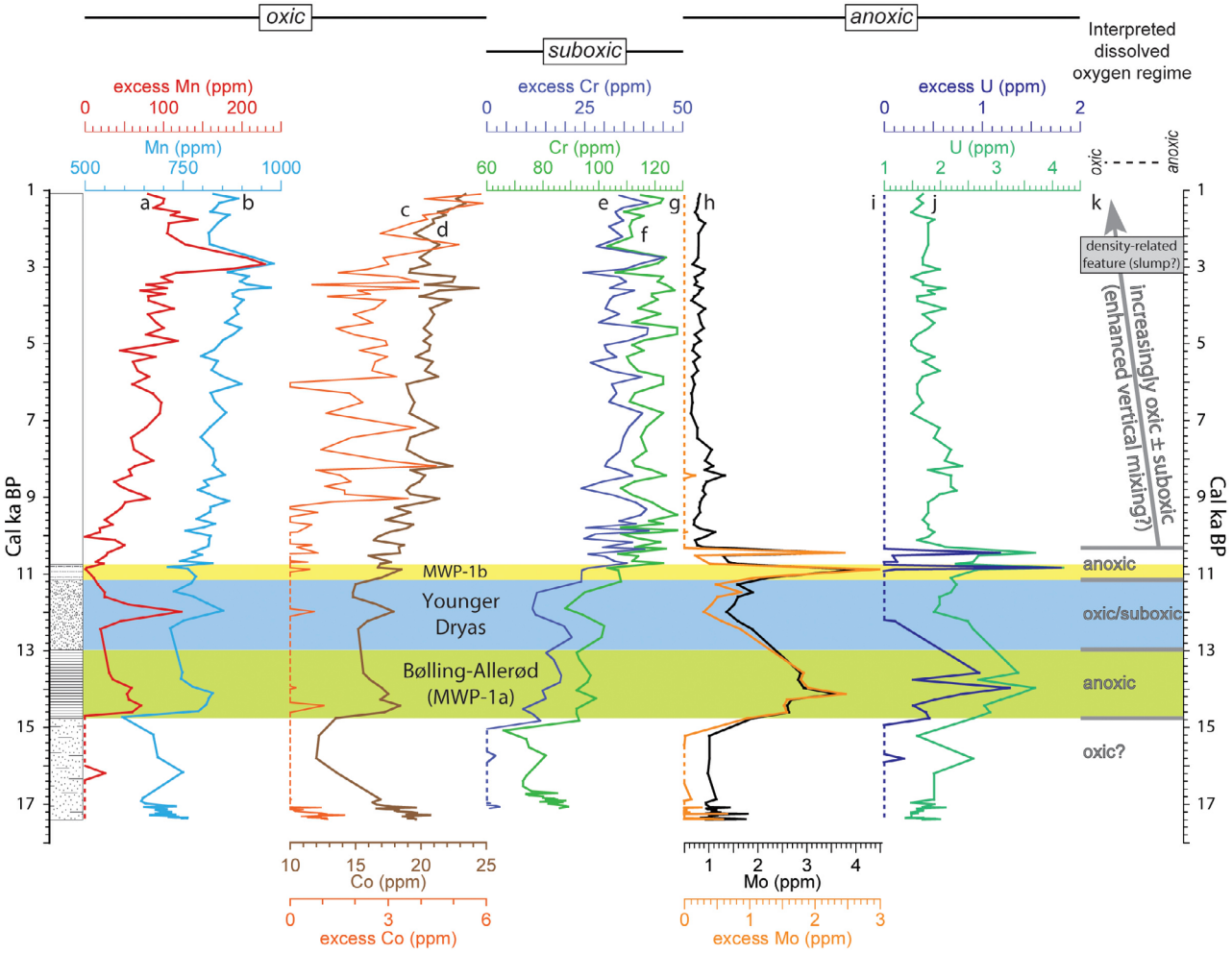

Figure 5. Redox-sensitive trace element proxies for dissolved oxygen regimes in EW0408–85JC. Enrichments of both (a) excess Mn and (b) total Mn and (c) excess Co and (d) total Co are associated with oxic conditions. (e) Excess Cr and (f) total Cr accumulation are sensitive to suboxia. (g) Excess Mo and (h) total Mo are indicative of suboxic-to-anoxic conditions, while anoxia is inferred from (i) excess U and (j) total U. (k) An interpreted dissolved oxygen regime index based on these data is also shown. Dashed lines indicate excess concentrations <0 ppm. Lithology patterns same as Figure 2.

Table 2. Calculated $\delta^{15}N_{marine}$ Values for EW0408–85JC Chronozones From Equations (5) and (7), Using Minimum, Mean, and Maximum Terrestrial and Marine End-Member Compositions, as Well as Forcing a Mean Holocene Value of 5‰

	Holocene	MWP-1b	Younger Dryas	Bølling-Allerød (MWP-1a)	Late Glacial Interval[a]
			Organic Matter $\delta^{13}C$		
Minimum	7.9 ± 2.9	10.6 ± 0.7	7.3 ± 1.4	8.5 ± 0.9	*
Mean	8.0 ± 1.8	11.5 ± 0.4	8.3 ± 1.3	9.5 ± 0.8	*
Maximum	8.4 ± 1.6	12.2 ± 0.3	9.1 ± 1.3	10.3 ± 0.7	11.1 ± 4.7
Holocene $\delta^{15}N$ = 5‰	5.0 ± 0.9	7.5 ± 0.2	5.7 ± 0.8	6.3 ± 0.4	5.7 ± 2.0
			Molar N/C Ratio		
Minimum	7.3 ± 1.7	5.7 ± 0.3	7.2 ± 2.3	9.1 ± 1.2	8.3 ± 78.5
Mean	7.6 ± 0.9	7.7 ± 0.4	8.2 ± 1.4	10.1 ± 0.8	10.4 ± 4.5
Maximum	8.1 ± 0.8	8.9 ± 0.5	9.0 ± 1.1	10.8 ± 0.7	8.8 ± 1.7
Holocene $\delta^{15}N$ = 5‰	5.0 ± 0.6	6.4 ± 0.2	5.8 ± 0.5	6.8 ± 0.4	4.9 ± 0.9

[a]Asterisks indicate that values were excluded because they approach end-member composition.

Holocene conditions favored enhanced primary productivity relative to LGI levels (Figure 2), reflected by higher concentrations of opal, TOC_{marine}, and excess Cd as well as the lower percentage of terrestrially derived OM.

[29] Holocene sedimentary $\delta^{15}N$ and $\delta^{13}C$ values (Figure 4) are higher than in LGI sediments. This difference reflects the greater contribution of terrigenous OM contained within the LGI sediments. Holocene $\delta^{15}N$ data are similar to modern marine nitrate $\delta^{15}N$ (4.1 ± 0.9‰) measured near Vancouver Island [*Wu et al.*, 1997] and global oceanic mean nitrate $\delta^{15}N$ (5‰) [*Galbraith et al.*, 2008b], but would be higher when corrected for dilution by terrestrial OM (Table 2). Observations from multiple high-export-productivity margins indicate bulk sedimentary $\delta^{15}N$ has an excellent correlation with local sub-euphotic zone nitrate $\delta^{15}N$ [*Altabet and Francois*, 1994; *Thunell et al.*, 2004]. Therefore, early Holocene $\delta^{15}N$ values between 10.7 and 7.0 cal ka BP appear to record an increase in fractional nitrate utilization by primary producers. High nitrate utilization (and hence high productivity) is suggested by the correspondence of high opal concentrations and high sedimentary $\delta^{15}N$ values.

4.1.3. Variations in Organic Matter $\delta^{13}C$, Sedimentary $\delta^{15}N$, and the Molar N/C Ratio: Proxy for Holocene Alaska Coastal Current Variability

[30] Similar patterns of change in sedimentary $\delta^{13}C$, $\delta^{15}N$, and molar N/C ratio data after 7.0 cal ka BP, during an interval of fairly constant opal MAR, suggest similar changes in organic matter composition independent of marine productivity contributions (Figure 4). Low $\delta^{15}N$ values between 6 to 3 cal ka BP can be explained by two mechanisms: (1) increased contributions of terrigenous OM, which is consistent with the sedimentary $\delta^{13}C$ and N/C ratio trends; or (2) incomplete nitrate utilization that limits export productivity. Increased N-fixation can also result in decreased $\delta^{15}N$ values [*Carpenter et al.*, 1997], but modern circulation patterns in the North Pacific Ocean argue against increased N-fixation as evidenced by: (1) negative N* values throughout the water column of the Subarctic Northeast Pacific [*Gruber and Sarmiento*, 1997; *Sarmiento and Gruber*, 2006] and (2) high nitrate concentrations measured directly in the Alaska Gyre and along the adjacent Gulf of Alaska shelf [*Childers et al.*, 2005]. Given these modern N-cycle constraints, and the synchronicity of the mid- and late Holocene fluctuations in sedimentary $\delta^{13}C$, $\delta^{15}N$, and molar N/C ratio data, these cycles likely represent discrete periods of enhanced terrigenous sediment delivery along the Gulf of Alaska slope.

[31] The proximity of the EW0408–85JC site to both the Copper River delta and the terminus of the Bering Glacier suggests both fluvial and glaciomarine processes contribute terrigenous sediment. While the Bering Glacier is the nearest potential glacial transport system, the Holocene advance and retreat record does not correspond to the enhanced terrestrial OM delivery during the mid-Holocene [*Molnia and Post*, 1995; *Wiles et al.*, 1999; *Calkin et al.*, 2001]. Modern satellite imagery shows distinctive sediment plumes transported westward by the Alaska Coastal Current along the northern Gulf of Alaska shelf (Figure 1c). These plumes are driven primarily by summer meltwater discharge originating in Icy and Yakutat Bays, as well as winter winds [*Stabeno et al.*, 2004]. Surface sediments from this area are characteristically rich in terrigenous OM [*Walinsky et al.*, 2009]. Therefore, changes in the delivery of glaciomarine sediment by the Alaska Coastal Current appear to be the most likely source of the millennial-scale shifts in terrigenous OM preserved in EW0408–85JC.

4.1.4. Trace Metal Evidence for Enhanced Holocene Vertical Mixing?

[32] Beginning at 10.7 cal ka BP, a monotonic increase in excess Mn concentrations corresponds with no accumulation of excess U or Mo (Figure 5). These patterns are disrupted during: (1) peaks in U, Mo, and Cd at 10.5 cal ka BP; and (2) a maximum in excess Mn around 3.0 cal ka BP that is synchronous with a CT density peak (Figure 2).

[33] Significant correlations exist between excess Mn and excess Fe ($n = 83$, $r = 0.57$, $p < 0.01$), excess Co ($n = 63$, $r = 0.47$, $p < 0.01$), and excess Cr ($n = 83$, $r = 0.26$, $p < 0.05$), suggesting association with Fe-Mn oxyhydroxide accumulation [*Tribovillard et al.*, 2006]. Oxic conditions favor dissolved Co^{2+} adsorption, precipitation of solid Co_3O_4 [*Brookins*, 1988] or $CoFe_2O_4$ [*Glasby and Schulz*, 1999], and/or complexation with organic ligands [*Saito et al.*, 2002]. Oxidized Cr^{6+} persists dominantly as aqueous CrO_4^{2-} in seawater, but is reduced to Cr^{3+} under suboxic conditions which then favors either the precipitation of solid Cr_2O_3 or the particle-reactive (aqua)hydroxyl cations $Cr(OH)_2^+$, $Cr(OH)_3$, and $(Cr, Fe)(OH)_3$. [*Calvert and Pedersen*, 1993; *Tribovillard et al.*, 2006]. While both Cr and Co-bearing sulfides are predicted to be thermodynamically stable in anoxic conditions, empirical data from a variety of marine depocenters suggests the kinetics of such reactions are too slow to result in significant enrichments [*Huerta-Diaz and Morse*, 1992; *Morse and Luther*, 1999].

[34] Increases in oxic-indicator trace elements (e.g., Mn and Co) in the Holocene section (Figure 5) suggest that the Holocene Gulf of Alaska continental slope has become progressively more oxygen-rich since the early Holocene. This increasingly oxic bottom water may be related to a number of factors, including enhanced vertical mixing, better ventilation of deep waters, or reduced remineralization rates of sinking particles. The increases in these oxic and suboxic indicator elements is not paralleled by trends in the productivity indicators (opal, TOC, and excess Cd; Figure 2), indicating the processes leading to the accumulation of these oxic indicators are likely independent of marine productivity. Thus, the lack of Holocene enrichments in Mo and U, and some precipitation of authigenic Mn, Co, and Cr, indicate at least suboxic bottom water conditions [*Calvert and Pedersen*, 1993; *Tribovillard et al.*, 2006], trending toward more oxic conditions since 10.7 cal ka BP.

4.2. The Bølling-Allerød in the Northern Gulf of Alaska

[35] The Bølling-Allerød interval begins at about 14.7 cal ka BP in the North Atlantic region [*Steffensen et al.*, 2008]. At this time, biogenic opal and TOC_{marine} concentrations double abruptly relative to LGI values, and Cd concentrations are at least three times higher (Figure 2). B-A sedimentary $\delta^{15}N$ values are also 3‰ higher than during the LGI (Figure 4). The combined presence of elevated concentrations of Mo and U, low concentrations of Mn, Co, and Cr (Figure 5), as well as the presence of laminated sediments, all indicate dysoxic-to-anoxic bottom water conditions.

[36] High concentrations of opal, TOC, and Cd (Figure 2) in B-A sediments indicate that productivity was higher. This inference is supported by increased percentages of the diatom *Thalassionema nitzschioides* and the silicoflagellate *Distephanus speculum* [*Barron et al.*, 2009]. Enhanced productivity during the B-A likely resulted in high export of OM to the benthos, remineralization of sinking particles within the water column and sediments, and low bottom water oxygen concentrations.

4.2.1. N Cycle Variability and Micronutrient Availability During the Bølling-Allerød (MWP-1a) and MWP-1b

[37] *Davies et al.* [2011] show that two intervals of laminated, opal-rich sediments record episodes of productivity in EW0408–85JC at 14.8 to 13 cal ka BP, and 11.2 to 10.8 cal ka BP, that correspond with the regional expressions of Meltwater Pulses (MWP-1a and −1b) [*Fairbanks*, 1989; *Kienast et al.*, 2003]. Davies et al. proposed that these periods of enhanced productivity in the Gulf of Alaska and other sites in the North Pacific resulted from episodes of abrupt sea level rise that inundated LGI coastal regions and mobilized labile bio-reactive micronutrients. Because the Gulf of Alaska is a major HNLC region with documented iron limitation of phytoplankton [e.g., *Boyd et al.*, 2004], and the EW0408–85JC core site lies on the modern boundary between the HNLC Alaska Gyre and the macronutrient-limited coastal zone [*Childers et al.*, 2005], we focus the discussion below on relationships between iron, the N cycle, and primary productivity in light of the MWP Fe availability hypothesis.

4.2.2. Distinguishing Between Refractory and Autochthonous $\delta^{15}N$ Signals

[38] The B-A interval in EW0408–85JC contains sedimentary $\delta^{15}N$ values of 5.7 ± 0.3‰, which exceed both the modern mean global nitrate $\delta^{15}N$ value of 5‰ [*Galbraith et al.*, 2008b] and deep North Pacific nitrate $\delta^{15}N$ value of 4.1 ± 0.9‰ [*Wu et al.*, 1997]. The m_{terr} calculations performed in section 3.2 (Figure 4) show that EW0408–85JC sedimentary OM is composed of a combination of terrigenous and marine sources, and because terrestrial $\delta^{15}N$ contributions can lower the bulk $\delta^{15}N$, it is necessary to correct the bulk $\delta^{15}N$ for better comparison to other North Pacific records to evaluate controls on $\delta^{15}N$ variability.

[39] We revise our earlier linear mixing model,

$$\delta^{15}N_{marine} = [\delta^{15}N_{sample} - (m_{terr} \times \delta^{15}N_{terr})]/m_{marine}, \quad (7)$$

where $m_{marine} = 1 - m_{terr}$, to solve for the $\delta^{15}N$ of bulk marine OM ($\delta^{15}N_{marine}$), where m_{terr} was determined using equation (5) (Table 1). Estimates of $\delta^{15}N_{marine}$ can be calculated using either the organic $\delta^{13}C$- or molar N/C-based solutions for m_{terr}. However, an estimate of this term is insufficient to calculate $\delta^{15}N_{marine}$, because equation (7) is under-determined with respect to the number of unknown end-member values necessary for a unique solution (i.e., A_{terr}, A_{marine} for either $\delta^{13}C$ or N/C in equation (5), and $\delta^{15}N_{terr}$ in equation (7)). Another shortcoming of this approach is that these carbon-based estimates of m_{terr} are dependent upon a fixed N:C value for the terrestrial OM end-member [e.g., *Meyers*, 1994]. Furthermore, as terrestrial OM tends to be depleted in N relative to marine OM, small changes in N content can produce large changes in N/C values [*Perdue and Koprivnjak*, 2007], and thus large potential variations in m_{terr}.

[40] To address these complications, $\delta^{15}N_{marine}$ was calculated using both the OM $\delta^{13}C$ and the molar N/C ratio, each in four different ways (Table 1): (1) maximum end-member composition values, so as to calculate the highest potential $\delta^{15}N_{marine}$ values; (2) minimum end-member compositions to determine the lowest potential $\delta^{15}N_{marine}$ values; (3) mean end-member values to derive a mean $\delta^{15}N_{marine}$ record; and (4) end-member values that were optimized to yield a mean Holocene $\delta^{15}N_{marine}$ of 5‰, which is equivalent to the modern value of mean oceanic nitrate $\delta^{15}N$ [*Galbraith et al.*, 2008b]. Given the level of uncertainty inherent in this approach, the $\delta^{15}N_{marine}$ calculations are best interpreted on a qualitative basis.

[41] The resultant $\delta^{15}N_{marine}$ estimations share several features (Table 2), including enriched $\delta^{15}N$ values during both the early Holocene and B-A. Some of the estimated values of $\delta^{15}N_{marine}$ during the LGI and the Holocene are high. In both cases, these unlikely results are due to measured compositions that approach the terrestrial or marine end-member compositions (Figure 4).

4.2.3. Enhanced Denitrification During the Bølling-Allerød? (Hypothesis 1)

[42] Considering the Holocene optimized $\delta^{13}C$ solution as the most conservative estimate for $\delta^{15}N_{marine}$ (Table 2) implies that the northern Gulf of Alaska continental slope experienced $\delta^{15}N_{marine} \geq 6.3$‰ during the B-A (MWP-1a), whereas the earliest Holocene (MWP-1b) saw $\delta^{15}N_{marine} \geq 7.5$‰. These values are analogous with those seen beneath the central Alaska Gyre at ODP Site 887 [*Galbraith et al.*, 2008a] and along the Vancouver shelf in core MD02–2496 [*Chang et al.*, 2008] during these same time intervals (Figure 6). However,

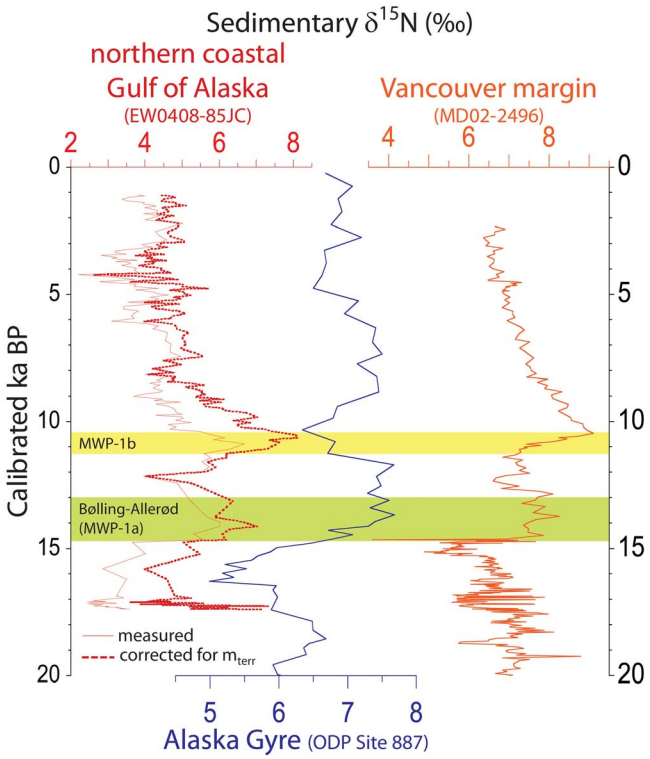

Figure 6. Regional bulk sedimentary δ^{15}N values from the Gulf of Alaska and Vancouver margin. EW0408–85JC values shown are the measured bulk δ^{15}N, as well as the marine δ^{15}N values corrected for terrestrial δ^{15}N input (calculated using the organic matter δ^{13}C values in equations (5) and (7), and optimized to yield a mean Holocene marine δ^{15}N = 5‰).

these records have not been corrected for terrestrially derived δ^{15}N contributions, and if significant, would lead to higher δ^{15}N values. For example, in MD02–2496 terrestrially derived organic C may be as high as 30% of the TOC content during the B-A [*Chang et al.*, 2008]. Comparisons with Arabian Sea [*Altabet et al.*, 2005] and eastern Equatorial Pacific δ^{15}N records [*Ganeshram et al.*, 1995; *Ganeshram et al.*, 2000], as well as particulate OM in the Black Sea [*Çoban-Yildiz et al.*, 2006], where water column denitrification has led to δ^{15}N enrichments of >9‰, suggests relatively weak denitrification may be affecting the Northeast Pacific records during both the B-A and early Holocene. In the case of EW0408–85JC, the B-A evidence of high biological productivity, intense water column anoxia, and preserved sedimentary laminations are consistent with water column conditions leading to denitrification [*Froelich et al.*, 1979], and thus elevated sedimentary δ^{15}N values [*Galbraith et al.*, 2008b]. A similar conclusion was reached by *Brunelle et al.* [2007, 2010] to explain the co-occurrence of suboxia, elevated diatom-bound δ^{15}N, and enriched sedimentary δ^{15}N in both the Bering Sea and the Sea of Okhotsk, with the added caveat that a nitrate utilization response in the δ^{15}N data may be indistinguishable from weak denitrification.

4.2.4. Supply of δ^{15}N-Enriched Nitrate From the Equatorial Pacific to the Gulf of Alaska? (Hypothesis 2)

[43] A second potential hypothesis to explain elevated δ^{15}N during the B-A and the earliest Holocene has been proposed by *Calvert et al.* [2001], namely that relatively enriched sedimentary δ^{15}N observed in Saanich Inlet sediment during the Holocene/LGI transition on Vancouver Island at ODP Site 1033 may be due to an isotopically heavier nitrate substrate being imported into the Northeast Pacific from the low latitude Equatorial Pacific margin. This model has also been invoked for linking Pacific sedimentary δ^{15}N maxima during the B-A interval, found on the continental shelves of Mexico, California, Oregon, and Canada [*Ganeshram et al.*, 1995; *Kienast et al.*, 2002; *Chang et al.*, 2008]. The recent recognition of shallow California Undercurrent water near the Aleutian Islands [*Thomson and Krassovski*, 2010] suggests that such a pathway is possible, but it is only a very small proportion of the total water column (~20% of the waters between 175 and 225 m depth in the northern Gulf of Alaska). Substantial flow of the California Undercurrent into the Gulf of Alaska in sizable volumes to cause the observed δ^{15}N enrichments seen in EW0408–85JC would require major and unlikely changes to North Pacific circulation, particularly a weakening of the North Pacific Current and the North Pacific Drift wind belt.

[44] Recent modeling of the North Pacific response to abrupt cooling initiated by freshwater hosing in the North Atlantic suggests there is a potential for weakening of the Aleutian Low and the associated North Pacific Drift during B-A warming [*Okumura et al.*, 2009]. Because this atmosphere-ocean linkage controls the intensity of the offshore "bifurcation" that occurs along the Vancouver coast, and gives rise to both the California Current and the Alaska Current (Figure 1a), weakening of the North Pacific Current would most likely diminish transport of preformed California Undercurrent nitrate northward. This mechanism would also require enhanced Alaska Gyre upwelling and advection to maintain the water mass balance in the Gulf of Alaska, which requires intensification of the Aleutian Low atmospheric cell and seems unlikely given the co-occurrence of seasonal sea-ice at this time (see below). The B-A planktonic foraminiferal δ^{13}C isotope record of *Davies et al.* [2011] also fails to support this hypothesis, in that the δ^{13}C values become anomalously heavy during this interval, suggesting that there was little influence of deep, upwelled waters at the EW0408–85JC site.

4.2.5. Relaxation of Micronutrient Limitation in the HNLC Gulf of Alaska (Hypothesis 3)

[45] A final potential hypothesis to explain the enriched δ^{15}N trends seen along the Gulf of Alaska margin is a change in the regional nutrient inventory, possibly forced by global sea level rise. An important component of the sea level hypothesis of *Davies et al.* [2011] is that during MWP-1a, the 13.5 – 24 m increase in sea level that occurred in less than 500 years [*Bard et al.*, 1990; *Blanchon and Shaw*, 1995; *Hanebuth et al.*, 2000] released labile bio-limiting micronutrients stored in subaerial LGI coastal zones. These micronutrients were then laterally advected offshore from the inundated continental shelf, and subsequent vertical mixing made these micronutrients available within the euphotic zone [*Chase et al.*, 2007; *Lam and Bishop*, 2008; *Severmann et al.*, 2010]. Because the Gulf of Alaska is a downwelling margin, and there is no evidence to suggest otherwise during the B-A [*Davies et al.*, 2011], then perhaps the locus of enhanced nitrate uptake favored by the relaxation of micronutrient

limitation was driven farther offshore than today. Higher nitrate utilization offshore resulted in an ^{15}N-enriched water mass advected into the coastal zone. This hypothesis favors enhanced nitrate uptake of the residual euphotic zone nitrate pool in areas traditionally considered micronutrient-limited, such as the open Gulf of Alaska.

[46] A second intense productivity and anoxia peak is observed between 11.2 – 10.7 cal ka BP (Figures 3 and 6). The timing of this peak occurs within MWP-1b identified in Barbados and Greenland [*Fairbanks*, 1989; *Steffensen et al.*, 2008], and corresponds to a somewhat smaller 12 m sea level rise [*Fairbanks*, 1990]. Dating of Tahitian corals, however, has recently cast doubt upon the rate and amplitude of MWP-1b [*Bard et al.*, 2010]. Nevertheless, the conceptual model described above to explain the relationship between sea level rise and North Pacific productivity may apply for the abrupt increase in $\delta^{15}N$ during MWP-1b (Figure 6). This period is further complicated by the inundation of the exposed Bering Sea continental shelf between 12.4 – 11.3 cal ka BP [*Keigwin et al.*, 2006] which could have affected ocean-atmosphere circulation and Fe release from shelf sediments.

4.3. Reconciling Productivity and Atmospheric Circulation in the Gulf of Alaska During the Bølling-Allerød: A Role for Sea Ice?

[47] The B-A Gulf of Alaska was probably cooler than today during boreal winter and may have contained seasonal sea ice despite inferred global B-A warming (Figure S2) [*de Vernal and Pedersen*, 1997; *Barron et al.*, 2009]. At about the same time, terrestrial glacier advances occurred [*Reger et al.*, 2008], and negative benthic foraminiferal $\delta^{18}O$ excursions potentially related to brine rejection are observed [*Davies et al.*, 2011]. Therefore, the B-A paleoenvironment along the northern Gulf of Alaska continental slope likely includes (1) enhanced export productivity that forced anoxia within the underlying water column; (2) enriched sedimentary $\delta^{15}N$ reflecting either weak denitrification or increased nitrate utilization due to greater micronutrient availability; (3) a dominantly downwelling circulation regime similar to modern conditions; (4) enhanced meltwater flux; and (5) seasonal sea ice. Many of these conditions no longer exist in the modern Gulf of Alaska.

[48] The presence of seasonal sea ice within the Northeast Pacific Ocean, southward to at least 54°N latitude (core PAR87A-10, Figure S2) [*de Vernal and Pedersen*, 1997] has potentially major implications for Gulf of Alaska primary productivity. In particular, sea ice would be a physical barrier to vertical mixing by winter storms, which now bring macronutrients present at depth into the euphotic zone for utilization by primary producers [*Childers et al.*, 2005]. The southward expansion of sea ice would also increase the regional albedo, thus altering the atmospheric heat budget and seasonal precipitation cycles. The Aleutian Low pressure cell is particularly sensitive to changes in the latitudinal temperature gradient [*Rind*, 1998], and high-latitude cooling can alter tropical and mid-tropical atmospheric convergence patterns [*Chiang and Bitz*, 2005; *Broccoli et al.*, 2006]. It is possible that the winter expansion of sea ice during the B-A in the Gulf of Alaska may have altered regional atmosphere-ocean dynamics, by forcing the Aleutian Low westward into a less intense configuration, as well as contributing to a weakened sea level pressure anomaly. Outputs from the NCAR Community Climate Model suggest that the winter Aleutian Low was indeed weakened during the B-A interval [*Bartlein et al.*, 1998]. Abundant winter sea ice thus may have lead to further deterioration of the Aleutian Low.

[49] Seasonal weakening of the modern Aleutian Low is associated with intensification and a northward shift of the North Pacific High along western North America [*Rodionov et al.*, 2007]. This mechanism leads to summer coastal upwelling in California and Oregon [*Hood et al.*, 1990]. A weakened Aleutian Low during the B-A interval was accompanied by intensified upwelling in the California Current as inferred from ODP Sites 1017 [*Hendy et al.*, 2004] and 1019 [*Barron et al.*, 2003], and elsewhere along the California margin [*Dean*, 2007], as a result of a strengthened North Pacific High. Weakened B-A Aleutian Low circulation has also been proposed on the basis of the Cave of the Bells stalagmite $\delta^{18}O$ record in the southwestern United States [*Wagner et al.*, 2010]. *Dean* [2007] proposed a model linking synchronous changes in productivity during the B-A along the western North America margin and in the Cariaco Basin, via atmospheric teleconnections in the Walker and Hadley circulation pathways that would affect the Aleutian Low and the subtropical high-pressure systems in both the North Pacific and the North Atlantic. Although the deglacial productivity peaks in the Gulf of Alaska are not a function of coastal upwelling, regional atmospheric reorganizations could provide a physical link between paleoclimate records in such widespread localities.

[50] Negative impacts on Gulf of Alaska primary productivity due to inferred B-A shifts in the Aleutian Low and the North Pacific High pressure cells were apparently counter-balanced by enhanced euphotic zone stratification forced by increased meltwater production from the retreating Cordilleran Ice Sheet and the occurrence of seasonal sea ice. Downwelling appears to be persistent throughout the EW0408–85JC record [*Davies et al.*, 2011], and these B-A changes in atmospheric boundary conditions may have increased downwelling relative to earlier LGI time, but less so than during the Holocene. The enhanced B-A marine productivity under weakened AL conditions is thus counter to traditional ecological models for the Gulf of Alaska [*Weingartner et al.*, 2002].

[51] Comparisons between the modern Bering Sea and the B-A Gulf of Alaska offer some insight into the sea ice – productivity linkage, with the caveat that the physiography of the two basins is markedly different and is reflected in the underlying physical oceanography that controls vertical mixing of deep nutrients into the euphotic zone [*Niebauer*, 1991; *Springer et al.*, 1996; *Stabeno et al.*, 1998, 2001, 2010]. Along the Bering Sea continental slope, exceedingly high primary productivity is augmented by two mechanisms specifically related to sea ice dynamics: (1) enhanced euphotic zone stratification that occurs due to the reduction in surface salinity during melting, and (2) mixing between macronutrient-rich offshore waters with iron-rich inshore waters, where the iron is derived from particulates released by the melting of sea ice [*Aguilar-Islas et al.*, 2008]. If further micronutrient reservoirs are needed to fully support the B-A Gulf of Alaska productivity maxima and high sedimentary $\delta^{15}N$ in EW0408–85JC, then rapid eustatic sea level rise and inundation of LGI coastal

regions (with release of iron from the flooded shelf regions) is a potential mechanism.

5. Conclusions

[52] Proxies for northern Gulf of Alaska productivity are consistently higher during the Bølling-Allerød and Holocene than during the Late Glacial Interval (LGI) and the Younger Dryas. The Bølling-Allerød interval is laminated and enriched in redox-sensitive elements, indicating productivity-driven dysoxic-to-anoxic bottom water conditions. These laminations are also associated with enriched sedimentary δ^{15}N ratios that indicate a link between productivity and N cycle dynamics.

[53] The synchronicity of the abrupt Bølling-Allerød transition in Greenland ice core records, several North Pacific continental margin sites, and the Cariaco Basin argues for a global forcing mechanism. Whereas EW0408–85JC was influenced by proximity to the Cordilleran Ice Sheet, most other Bølling-Allerød records of heightened productivity from the North Pacific are far removed from glacial margins. Many of these other records can be explained by changes in upwelling intensity, but the Gulf of Alaska paleocirculation is more consistent with downwelling conditions.

[54] The sea level hypothesis outlined by *Davies et al.* [2011] provides a testable framework within which to evaluate our proxy results from EW0408–85JC in the greater context of North Pacific paleoceanographic records. The unique location of EW0408–85JC allows us to simultaneously eliminate both glacial activity and upwelling from the potential mechanisms that lead to the North Pacific productivity increase during the Bølling-Allerød. Instead, the rapid inundation of LGI coastal regions worldwide during periods of abrupt sea level rise appears as a strong candidate for explaining this productivity phenomenon. As labile bio-reactive micronutrients were mobilized from LGI estuaries and advected into the coastal euphotic zone, the micronutrient limitation of North Pacific HNLC water was alleviated and large-scale productivity blooms were initiated along much of the margin. In turn, the export of this autochthonous organic material then led to the onset of anoxic conditions within the underlying water column and sediment, thus enabling the preservation of laminations at slope depths throughout the North Pacific. This model is further supported by our sedimentary δ^{15}N data. The mildly enriched δ^{15}N observed along the Gulf of Alaska margin during the Bølling-Allerød suggests a change in the locus of the micronutrient-limited HNLC front farther seaward, with subsequent advection of ^{15}N-enriched nitrate into the coastal zone, though intense productivity leading to water column denitrification may have also played a role.

[55] **Acknowledgments.** We thank the crew and scientific party of cruise EW0408 onboard the R/V *Maurice Ewing*, as well as Bobbi Conard and Mysti Weber of the Oregon State University core repository. Analytical assistance provided by Andrea Krumhardt, Tara Borland, Jamie Coon, and Jennifer Addison was invaluable, as was the support of the Alaska Stable Isotope Facility. The manuscript benefited greatly from discussions with Fred Prahl, John Barron, and Lesleigh Anderson. Sedimentary δ^{15}N data from ODP Site 887 and MD02–2496 were provided by Eric Galbraith and Alice Chang, respectively. This publication results in part from a UAF Center for Global Change Student Award to J.A.A. funded by the Cooperative Institute for Arctic Research through cooperative agreement NA17RJ1224 with the National Oceanic and Atmospheric Administration. B.P.F. was supported through NSF grant OCE-0351075. W.E.D. was supported by the USGS Earth Surface Dynamics Program. Editorial comments provided by Rainer Zahn, Alexander van Geen, and an anonymous reviewer greatly improved this manuscript.

References

Aguilar-Islas, A. M., R. D. Rember, C. W. Mordy, and J. Wu (2008), Sea ice-derived dissolved iron and its potential influence on the spring algal bloom in the Bering Sea, *Geophys. Res. Lett.*, *35*, L24601, doi:10.1029/2008GL035736.

Aitchison, J. (1986), *The Statistical Analysis of Compositional Data*, 416 pp., Chapman and Hall, London, doi:10.1007/978-94-009-4109-0.

Aitchison, J. (1999), Logratios and natural laws in compositional data analysis, *Math. Geol.*, *31*(5), 563–580, doi:10.1023/A:1007568008032.

Altabet, M. A., and R. Francois (1994), Sedimentary nitrogen isotopic ratio as a recorder for surface ocean nitrate utilization, *Global Biogeochem. Cycles*, *8*(1), 103–116, doi:10.1029/93GB03396.

Altabet, M. A., R. Agnihotri, J. Tierny, S. M. Higgins, and T. D. Herbert (2005), A tale of two margins: A comparison of redox and productivity paleo-proxies in sediments off Oman and Peru, *Geochim. Cosmochim. Acta*, *69*(10), A578–A578.

Bard, E., B. Hamelin, and R. G. Fairbanks (1990), U-Th ages obtained by mass-spectrometry in corals from Barbados: Sea level during the past 130,000 years, *Nature*, *346*(6283), 456–458, doi:10.1038/346456a0.

Bard, E., B. Hamelin, and D. Delanghe-Sabatier (2010), Deglacial Meltwater Pulse 1B and Younger Dryas sea levels revisited with boreholes at Tahiti, *Science*, *327*, 1235–1237, doi:10.1126/science.1180557.

Barron, J. A., L. Heusser, T. Herbert, and M. Lyle (2003), High-resolution climatic evolution of coastal northern California during the past 16,000 years, *Paleoceanography*, *18*(1), 1020, doi:10.1029/2002PA000768.

Barron, J. A., D. Bukry, W. E. Dean, J. A. Addison, and B. P. Finney (2009), Paleoceanography of the Gulf of Alaska during the past 15,000 years: Results from diatoms, silicoflagellates, and geochemistry, *Mar. Micropaleontol.*, *72*, 176–195, doi:10.1016/j.marmicro.2009.04.006.

Bartlein, P. J., K. H. Anderson, P. M. Anderson, M. E. Edwards, C. J. Mock, R. S. Thompson, R. S. Webb, and C. Whitlock (1998), Paleoclimate simulations for North America over the past 21,000 years: Features of the simulated climate and comparisons with paleoenvironmental data, *Quat. Sci. Rev.*, *17*(6–7), 549–585, doi:10.1016/S0277-3791(98)00012-2.

Blanchon, P., and J. S. Shaw (1995), Reef drowning during the last deglaciation: Evidence for catastrophic sea-level rise and ice-sheet collapse, *Geology*, *23*, 4–8, doi:10.1130/0091-7613(1995)023<0004:RDDTLD>2.3.CO;2.

Blum, P. (1997), Physical properties handbook: A guide to the shipboard measurement of physical properties of deep-sea cores, *ODP Tech. Note 26*, Integr. Ocean Drill. Program, New York, doi:10.2973/odp.tn.26.1997.

Boyd, P. W., et al. (2004), The decline and fate of an iron-induced subarctic phytoplankton bloom, *Nature*, *428*(6982), 549–553, doi:10.1038/nature02437.

Broccoli, A. J., K. A. Dahl, and R. J. Stouffer (2006), Response of the ITCZ to Northern Hemisphere cooling, *Geophys. Res. Lett.*, *33*, L01702, doi:10.1029/2005GL024546.

Brookins, D. G. (1988), *Eh-pH Diagrams for Geochemistry*, 176 pp., Springer, Berlin.

Bruland, K. W., E. L. Rue, and G. J. Smith (2001), Iron and macronutrients in California coastal upwelling regimes: Implications for diatom blooms, *Limnol. Oceanogr.*, *46*(7), 1661–1674, doi:10.4319/lo.2001.46.7.1661.

Brunelle, B. G., D. M. Sigman, M. S. Cook, L. D. Keigwin, G. H. Haug, B. Plessen, G. Schettler, and S. L. Jaccard (2007), Evidence from diatom-bound nitrogen isotopes for subarctic Pacific stratification during the last ice age and a link to North Pacific denitrification changes, *Paleoceanography*, *22*, PA1215, doi:10.1029/2005PA001205.

Brunelle, B. G., D. M. Sigman, S. L. Jaccard, L. D. Keigwin, B. Plessen, G. Schettler, M. S. Cook, and G. H. Haug (2010), Glacial/interglacial changes in nutrient supply and stratification in the western subarctic North Pacific since the penultimate glacial maximum, *Quat. Sci. Rev.*, *29*, 2579–2590, doi:10.1016/j.quascirev.2010.03.010.

Caissie, B. E., J. Brigham-Grette, K. T. Lawrence, T. D. Herbert, and M. S. Cook (2010), Last Glacial Maximum to Holocene sea surface conditions at Umnak Plateau, Bering Sea, as inferred from diatom, alkenone, and stable isotope records, *Paleoceanography*, *25*, PA1206, doi:10.1029/2008PA001671.

Calkin, P. E., G. C. Wiles, and D. J. Barclay (2001), Holocene coastal glaciation of Alaska, *Quat. Sci. Rev.*, *20*(1–3), 449–461, doi:10.1016/S0277-3791(00)00105-0.

Calvert, S. E., and T. F. Pedersen (1993), Geochemistry of recent oxic and anoxic marine sediments: Implications for the geological record, *Mar. Geol.*, *113*(1–2), 67–88, doi:10.1016/0025-3227(93)90150-T.

Calvert, S. E., T. F. Pedersen, and R. E. Karlin (2001), Geochemical and isotopic evidence for post-glacial palaeoceanographic changes in Saanich

Inlet, British Columbia, *Mar. Geol.*, *174*(1–4), 287–305, doi:10.1016/S0025-3227(00)00156-0.

Carpenter, E. J., H. R. Harvey, B. Fry, and D. G. Capone (1997), Biogeochemical tracers of the marine cyanobacterium Trichodesmium, *Deep Sea Res., Part I*, *44*(1), 27–38, doi:10.1016/S0967-0637(96)00091-X.

Chang, A. S., T. F. Pedersen, and I. L. Hendy (2008), Late Quaternary paleoproductivity history on the Vancouver Island margin, western Canada: A multiproxy geochemical study, *Can. J. Earth Sci.*, *45*, 1283–1297, doi:10.1139/E08-038.

Chase, Z., P. G. Strutton, and B. Hales (2007), Iron links river runoff and shelf width to phytoplankton biomass along the U.S. West Coast, *Geophys. Res. Lett.*, *34*, L04607, doi:10.1029/2006GL028069.

Chiang, J. C. H., and C. M. Bitz (2005), Influence of high latitude ice cover on the marine Intertropical Convergence Zone, *Clim. Dyn.*, *25*(5), 477–496, doi:10.1007/s00382-005-0040-5.

Childers, A. R., T. E. Whitledge, and D. A. Stockwell (2005), Seasonal and interannual variability in the distribution of nutrients and chlorophyll a across the Gulf of Alaska shelf: 1998–2000, *Deep Sea Res., Part II*, *52*(1–2), 193–216, doi:10.1016/j.dsr2.2004.09.018.

Coale, K. H., et al. (1996), A massive phytoplankton bloom induced by an ecosystem-scale iron fertilization experiment in the equatorial Pacific Ocean, *Nature*, *383*, 495–501, doi:10.1038/383495a0.

Çoban-Yildiz, Y., M. A. Altabet, A. Yilmaz, and S. Tugrul (2006), Carbon and nitrogen isotopic ratios of suspended particulate organic matter (SPOM) in the Black Sea water column, *Deep Sea Res., Part II*, *53*(17–19), 1875–1892, doi:10.1016/j.dsr2.2006.03.021.

Conley, D. J. (1998), An interlaboratory comparison for the measurement of biogenic silica in sediments, *Mar. Chem.*, *63*, 39–48, doi:10.1016/S0304-4203(98)00049-8.

Cook, M. S., L. D. Keigwin, and C. A. Sancetta (2005), The deglacial history of surface and intermediate water of the Bering Sea, *Deep Sea Res., Part II*, *52*(16–18), 2163–2173, doi:10.1016/j.dsr2.2005.07.004.

Crusius, J., T. F. Pedersen, S. Kienast, L. Keigwin, and L. Labeyrie (2004), Influence of northwest Pacific productivity on North Pacific Intermediate Water oxygen concentrations during the Boiling-Allerod interval (14.7–12.9 ka), *Geology*, *32*(7), 633–636, doi:10.1130/G20508.1.

Crusius, J., A. W. Schroth, S. Gasso, C. M. Moy, R. C. Levy, and M. Gatica (2011), Glacial flour dust storms in the Gulf of Alaska: Hydrologic and meteorological controls and their importance as a source of bioavailable iron, *Geophys. Res. Lett.*, *38*, L06602, doi:10.1029/2010GL046573.

Davies, M. H., A. C. Mix, J. S. Stoner, J. A. Addison, J. M. Jaeger, B. P. Finney, and J. Wiest (2011), The deglacial transition on the Southeastern Alaska Margin: Meltwater input, sealevel rise, marine productivity, and sedimentary anoxia, *Paleoceanography*, *26*, PA2223, doi:10.1029/2010PA002051.

Davis, J. C. (2002), *Statistics and Data Analysis in Geology*, 3rd ed., 638 pp., John Wiley, New York.

Dean, W. E. (2007), Sediment geochemical records of productivity and oxygen depletion along the margin of western North America during the past 60,000 years: Teleconnections with Greenland Ice and the Cariaco Basin, *Quat. Sci. Rev.*, *26*(1–2), 98–114, doi:10.1016/j.quascirev.2006.08.006.

Dean, W. E., Y. Zheng, J. D. Ortiz, and A. van Geen (2006), Sediment Cd and Mo accumulation in the oxygen-minimum zone off western Baja California linked to global climate over the past 52 kyr, *Paleoceanography*, *21*, PA4209, doi:10.1029/2005PA001239.

Deschamps, P., N. Durand, E. Bard, B. Hamelin, G. Camoin, A. L. Thomas, G. M. Henderson, and Y. Yokoyama (2009), Synchroneity of Meltwater Pulse 1A and the Bolling onset: New evidence from the IODP "Tahiti Sea-Level" Expedition, *Geophys. Res. Abstr.*, *11*, EGU2009-10223.

de Vernal, A., and T. F. Pedersen (1997), Micropaleontology and palynology of core PAR87A–10: A 23,000 year record of paleoenvironmental changes in the Gulf of Alaska, northeast North Pacific, *Paleoceanography*, *12*(6), 821–830, doi:10.1029/97PA02167.

Engleman, E. E., L. L. Jackson, D. R. Norton, and A. G. Fischer (1985), Determination of carbonate carbon in geological materials by coulometric titration, *Chem. Geol.*, *53*, 125–128, doi:10.1016/0009-2541(85)90025-7.

Fairbanks, R. G. (1989), A 17,000-year glacio-eustatic sea-level record - influence of glacial melting rates on the Younger Dryas event and deep-ocean circulation, *Nature*, *342*(6250), 637–642, doi:10.1038/342637a0.

Fairbanks, R. G. (1990), The age and origin of the "Younger Dryas Climate Event" in Greenland ice cores, *Paleoceanography*, *5*(6), 937–948, doi:10.1029/PA005i006p00937.

Falkowski, P. G., R. T. Barber, and V. Smetacek (1998), Biogeochemical controls and feedbacks on ocean primary production, *Science*, *281*, 200–206, doi:10.1126/science.281.5374.200.

Francois, R., M. Frank, M. M. Rutgers van der Loeff, and M. P. Bacon (2004), ^{230}Th normalization: An essential tool for interpreting sedimentary fluxes during the late Quaternary, *Paleoceanography*, *19*, PA1018, doi:10.1029/2003PA000939.

Froelich, P. N., G. P. Klinkhammer, M. L. Bender, N. A. Luedtke, G. R. Heath, D. Cullen, P. Dauphin, D. E. Hammond, B. Hartmann, and V. Maynard (1979), Early oxidation of organic matter in pelagic sediments of the eastern equatorial Atlantic: Suboxic diagenesis, *Geochim. Cosmochim. Acta*, *43*, 1075–1090, doi:10.1016/0016-7037(79)90095-4.

Galbraith, E. D., S. L. Jaccard, T. F. Pedersen, D. M. Sigman, G. H. Haug, M. Cook, J. R. Southon, and R. Francois (2007), Carbon dioxide release from the North Pacific abyss during the last deglaciation, *Nature*, *449*, 890–893, doi:10.1038/nature06227.

Galbraith, E. D., M. Kienast, S. L. Jaccard, T. F. Pedersen, B. G. Brundle, and T. Kiefer (2008a), Consistent relationship between global climate and surface nitrate utilization in western Subarctic Pacific throughout the last 500 ky, *Paleoceanography*, *23*, PA2212, doi:10.1029/2007PA001518.

Galbraith, E. D., D. M. Sigman, R. S. Robinson, and T. F. Pedersen (2008b), Nitrogen in past marine environments, in *Nitrogen in the Marine Environment*, edited by D. G. Capone et al., pp. 1497–1535, Academic, San Diego, Calif, doi:10.1016/B978-0-12-372522-6.00034-7.

Ganeshram, R. S., T. F. Pedersen, S. E. Calvert, and J. W. Murray (1995), Large changes in oceanic nutrient inventories from glacial to interglacial periods, *Nature*, *376*(6543), 755–758, doi:10.1038/376755a0.

Ganeshram, R. S., T. F. Pedersen, S. E. Calvert, G. W. McNeill, and M. R. Fontugne (2000), Glacial-interglacial variability in denitrification in the world's oceans: Causes and consequences, *Paleoceanography*, *15*(4), 361–376, doi:10.1029/1999PA000422.

Garcia, H. E., R. A. Locarnini, T. P. Boyer, and J. I. Antonov (2006), *World Ocean Atlas 2005*, vol. 4, *Nutrients (Phosphate, Nitrate, and Silicate)*, *NOAA Atlas NESDIS*, vol. 64, edited by S. Levitus, 396 pp., NOAA, Silver Spring, Md.

Gargett, A. E. (1997), The optimal stability 'window': A mechanism underlying decadal fluctuations in North Pacific salmon stocks?, *Fish. Oceanogr.*, *6*(2), 109–117, doi:10.1046/j.1365-2419.1997.00033.x.

Gaye-Haake, B., et al. (2005), Stable nitrogen isotopic ratios of sinking particles and sediments from the northern Indian Ocean, *Mar. Chem.*, *96*(3–4), 243–255, doi:10.1016/j.marchem.2005.02.001.

Geider, R. J., and J. La Roche (2002), Redfield revisited: Variability of C:N:P in marine microalgae and its biochemical basis, *Eur. J. Phycol.*, *37*(1), 1–17, doi:10.1017/S0967026201003456.

Glasby, G. P., and H. D. Schulz (1999), Eh, pH diagrams for Mn, Fe, Co, Ni, Cu and As under seawater conditions: Application of two new types of Eh, pH diagrams to the study of specific problems in marine geochemistry, *Aquat. Geochem.*, *5*, 227–248, doi:10.1023/A:1009663322718.

Gruber, N., and J. L. Sarmiento (1997), Global patterns of marine nitrogen fixation and denitrification, *Global Biogeochem. Cycles*, *11*(2), 235–266, doi:10.1029/97GB00077.

Gulick, S., J. Jaeger, J. Freymueller, P. Koons, T. Pavlis, and R. D. Powell (2004), Examining tectonic-climatic interactions in Alaska and the Northeastern Pacific, *Eos Trans. AGU*, *85*(43), 433–448, doi:10.1029/2004EO430001.

Hanebuth, T. J. J., K. Stattegger, and P. M. Grootes (2000), Rapid flooding of the Sunda shelf: A late-glacial sea-level record, *Science*, *288*, 1033–1035, doi:10.1126/science.288.5468.1033.

Harrison, P. J., P. W. Boyd, D. E. Varela, and S. Takeda (1999), Comparison of factors controlling phytoplankton productivity in the NE and NW subarctic Pacific gyres, *Prog. Oceanogr.*, *43*(2–4), 205–234, doi:10.1016/S0079-6611(99)00015-4.

Hedges, J. I., F. S. Hu, A. H. Devol, H. E. Hartnett, E. Tsamakis, and R. G. Keil (1999), Sedimentary organic matter preservation: A test for selective degradation under oxic conditions, *Am. J. Sci.*, *299*(7–9), 529–555, doi:10.2475/ajs.299.7-9.529.

Hendy, I. L., and T. F. Pedersen (2005), Is pore water oxygen content decoupled from productivity on the California Margin? Trace element results from Ocean Drilling Program Hole 1017E, San Lucia slope, California, *Paleoceanography*, *20*, PA4026, doi:10.1029/2004PA001123.

Hendy, I. L., T. F. Pedersen, J. P. Kennett, and R. Tada (2004), Intermittent existence of a southern Californian upwelling cell during submillennial climate change of the last 60 kyr, *Paleoceanography*, *19*, PA3007, doi:10.1029/2003PA000965.

Hood, R. R., M. R. Abbott, A. Huyer, and P. M. Kosro (1990), Surface patterns in temperature, flow, phytoplankton biomass, and species composition in the coastal transition zone off northern California, *J. Geophys. Res.*, *95*(C10), 18,081–18,094, doi:10.1029/JC095iC10p18081.

Hopkins, D. M. (1959), Cenozoic history of the Bering Land Bridge, *Science*, *129*, 1519–1528, doi:10.1126/science.129.3362.1519.

Horikawa, K., Y. Asahara, K. Yamamoto, and Y. Okazaki (2010), Intermediate water formation in the Bering Sea during glacial periods: Evidence from neodymium isotope ratios, *Geology*, *38*(5), 435–438, doi:10.1130/G30225.1.

Huerta-Diaz, M. A., and J. W. Morse (1992), Pyritization of trace metals in anoxic marine sediments, *Geochim. Cosmochim. Acta*, *56*, 2681–2702, doi:10.1016/0016-7037(92)90353-K.

Ivanochko, T. S., and T. F. Pedersen (2004), Determining the influences of Late Quaternary ventilation and productivity variations on Santa Barbara Basin sedimentary oxygenation: A multi-proxy approach, *Quat. Sci. Rev.*, *23*, 467–480, doi:10.1016/j.quascirev.2003.06.006.

Jaeger, J. M., C. A. Nittrouer, N. D. Scott, and J. D. Milliman (1998), Sediment accumulation along a glacially impacted mountainous coastline: North-east Gulf of Alaska, *Basin Res.*, *10*(1), 155–173, doi:10.1046/j.1365-2117.1998.00059.x.

Johnson, W. K., L. A. Miller, N. E. Sutherland, and C. S. Wong (2005), Iron transport by mesoscale Haida eddies in the Gulf of Alaska, *Deep Sea Res., Part II*, *52*, 933–953, doi:10.1016/j.dsr2.2004.08.017.

Katsuki, K., B. K. Khim, T. Itaki, Y. Okazaki, K. Ikehara, Y. Shin, H. I. Yoon, and C. Y. Kang (2010), Sea-ice distribution and atmospheric pressure patterns in southwestern Okhotsk Sea since the Last Glacial Maximum, *Global Planet. Change*, *72*(3), 99–107, doi:10.1016/j.gloplacha.2009.12.005.

Kaufman, D., and W. F. Manley (2004), Pleistocene Maximum and Late Wisconsinan glacier extents across Alaska, U.S.A, in *Quaternary Glaciations - Extent and chronology, Part II: North America*, edited by J. Ehlers and P. L. Gibbard, pp. 9–27, Elsevier, Amsterdam.

Keigwin, L. D. (2002), Late Pleistocene-Holocene paleoceanography and ventilation of the Gulf of California, *J. Oceanogr.*, *58*, 421–432, doi:10.1023/A:1015830313175.

Keigwin, L. D., J. P. Donnelly, M. S. Cook, N. W. Driscoll, and J. Brigham-Grette (2006), Rapid sea-level rise and Holocene climate in the Chukchi Sea, *Geology*, *34*(10), 861–864, doi:10.1130/G22712.1.

Kienast, M., T. J. J. Hanebuth, C. Pelejero, and S. Steinke (2003), Synchroneity of meltwater pulse 1a and the Bolling warming: New evidence from the South China Sea, *Geology*, *31*(1), 67–70, doi:10.1130/0091-7613(2003)031<0067:SOMPAT>2.0.CO;2.

Kienast, S. S., S. E. Calvert, and T. F. Pedersen (2002), Nitrogen isotope and productivity variations along the northwest Pacific margin over the last 120 kyr, *Paleoceanography*, *17*(4), 1055, doi:10.1029/2001PA000650.

Kulm, L. D., R. von Huene, J. R. Duncan, J. C. Ingle, S. A. Kling, D. J. W. Piper, R. M. Pratt, H.-J. Scharder, S. W. Wise, and L. F. Musich (1973), Introduction, *Initial Rep. Deep Sea Drill. Proj.*, *18*, 5–8, doi:10.2973/dsdp.proc.18.1973.

Ladd, C., P. Stabeno, and E. D. Cokelet (2005), A note on cross-shelf exchange in the northern Gulf of Alaska, *Deep Sea Res., Part II*, *52*(5–6), 667–679, doi:10.1016/j.dsr2.2004.12.022.

Lam, P. J., and J. K. B. Bishop (2008), The continental margin is a key source of iron to the HNLC North Pacific Ocean, *Geophys. Res. Lett.*, *35*, L07608, doi:10.1029/2008GL033294.

Lane, T. W., and F. M. M. Morel (2000), A biological function for cadmium in marine diatoms, *Proc. Natl. Acad. Sci. U. S. A.*, *97*(9), 4627–4631, doi:10.1073/pnas.090091397.

Lane, T. W., M. A. Saito, G. N. George, I. J. Pickering, R. C. Prince, and F. M. M. Morel (2005), Biogeochemistry: A cadmium enzyme from a marine diatom, *Nature*, *435*(7038), 42, doi:10.1038/435042a.

Lee, J. G., S. B. Roberts, and F. M. M. Morel (1995), Cadmium: A nutrient for the marine diatom *Thalassiosira weissflogii*, *Limnol. Oceanogr.*, *40*(6), 1056–1063, doi:10.4319/lo.1995.40.6.1056.

Lynn, R. J., and J. J. Simpson (1987), The California Current System: The seasonal variability of its physical characteristics, *J. Geophys. Res.*, *92*(C12), 12,947–12,966, doi:10.1029/JC092iC12p12947.

Martin, J. H. (1990), Glacial-interglacial CO_2 change: The iron hypothesis, *Paleoceanography*, *5*, 1–13, doi:10.1029/PA005i001p00001.

Martin, J. H., and S. E. Fitzwater (1988), Iron deficiency limits phytoplankton growth in the north-east Pacific subarctic, *Nature*, *331*, 341–343, doi:10.1038/331341a0.

McDonald, D., T. F. Pedersen, and J. Crusius (1999), Multiple late Quaternary episodes of exceptional diatom production in the Gulf of Alaska, *Deep Sea Res., Part II*, *46*(11–12), 2993–3017, doi:10.1016/S0967-0645(99)00091-0.

McLennan, S. M. (1995), Sediments and soils: Chemistry and abundances, in *Rock Physics & Phase Relations: A Handbook of Physical Constants*, *AGU Ref. Shelf*, vol. 3, edited by T. J. Ahrens, pp. 8–19, AGU, Washington, D. C., doi:10.1029/RF003p0008

McQuoid, M. R., M. J. Whiticar, S. E. Calvert, and T. F. Pedersen (2001), A post-glacial isotope record of primary production and accumulation in the organic sediments of Saanich Inlet, ODP Leg 169S, *Mar. Geol.*, *174*(1–4), 273–286, doi:10.1016/S0025-3227(00)00155-9.

Meyers, P. A. (1994), Preservation of elemental and isotopic source identification of sedimentary organic matter, *Chem. Geol.*, *114*(3–4), 289–302, doi:10.1016/0009-2541(94)90059-0.

Molnia, B. F. (1982), Erosion, deposition, faulting, and instability of shelf sediments: Eastern Gulf of Alaska, in *Outer Continental Shelf Environmental Assessment Program, Final Reports of Principal Investigators*, *Rep. 3951*, 638 pp., U.S. Dep. of the Inter., Washington, D. C.

Molnia, B. F., and A. Post (1995), Holocene history of Bering Glacier, Alaska: A prelude to the 1993–1994 surge, *Phys. Geogr.*, *16*(2), 87–117.

Morel, F. M. M., and N. M. Price (2003), The biogeochemical cycles of trace metals in the oceans, *Science*, *300*, 944–947, doi:10.1126/science.1083545.

Morse, J. W., and G. W. Luther III (1999), Chemical influences on trace metal-sulfide interactions in anoxic sediments, *Geochim. Cosmochim. Acta*, *63*, 3373–3378, doi:10.1016/S0016-7037(99)00258-6.

Mortlock, R. A., and P. N. Froelich (1989), A simple method for the rapid determination of biogenic opal in pelagic marine sediments, *Deep Sea Res.*, *36*(9), 1415–1426, doi:10.1016/0198-0149(89)90092-7.

Nameroff, T. J., L. S. Balistrieri, and J. W. Murray (2002), Suboxic trace metal geochemistry in the eastern tropical North Pacific, *Geochim. Cosmochim. Acta*, *66*(7), 1139–1158, doi:10.1016/S0016-7037(01)00843-2.

Needoba, J. A., A. Marchetti, M. F. Henry, P. J. Harrison, C. S. Wong, W. K. Johnson, and T. F. Pedersen (2006), Stable nitrogen isotope dynamics of a mesoscale iron enrichment experiment in the NE Subarctic Pacific, *Deep Sea Res., Part II*, *53*(20–22), 2214–2230, doi:10.1016/j.dsr2.2006.05.021.

Niebauer, H. J. (1991), Bio-physical oceanographic interactions at the edge of the Arctic ice pack, *J. Mar. Syst.*, *2*, 209–232, doi:10.1016/0924-7963(91)90025-P.

Nishioka, J., S. Takeda, C. S. Wong, and W. K. Johnson (2001), Size-fractionated iron concentrations in the Northeast Pacific Ocean: Distribution of soluble and small colloidal iron, *Mar. Chem.*, *74*, 157–179, doi:10.1016/S0304-4203(01)00013-5.

Ohkushi, K., T. Itaki, and N. Nemoto (2003), Last Glacial-Holocene change in intermediate-water ventilation in the Northwestern Pacific, *Quat. Sci. Rev.*, *22*, 1477–1484, doi:10.1016/S0277-3791(03)00082-9.

Okazaki, Y., K. Takahashi, H. Asahi, K. Katsuki, J. Hori, H. Yasuda, Y. Sagawa, and H. Tokuyama (2005a), Productivity changes in the Bering Sea during the late Quaternary, *Deep Sea Res., Part II*, *52*(16–18), 2150–2162, doi:10.1016/j.dsr2.2005.07.003.

Okazaki, Y., K. Takahashi, K. Katsuki, A. Ono, J. Hori, T. Sakamoto, M. Uchida, Y. Shibata, M. Ikehara, and K. Aoki (2005b), Late Quaternary paleoceanographic changes in the southwestern Okhotsk Sea: Evidence from geochemical, radiolarian, and diatom records, *Deep Sea Res., Part II*, *52*(16–18), 2332–2350, doi:10.1016/j.dsr2.2005.07.007.

Okumura, Y. M., C. Deser, A. Hu, A. Timmermann, and S. P. Xie (2009), North Pacific climate response to freshwater forcing in the Subarctic North Atlantic: Oceanic and atmospheric pathways, *J. Clim.*, *22*(6), 1424–1445, doi:10.1175/2008JCLI2511.1.

Perdue, E. M., and J. F. Koprivnjak (2007), Using the C/N ratio to estimate terrigenous inputs of organic matter to aquatic environments, *Estuarine Coastal Shelf Sci.*, *73*(1–2), 65–72, doi:10.1016/j.ecss.2006.12.021.

Peteet, D. M., and D. H. Mann (1994), Late-glacial vegetational, tephra, and climatic history of southwestern Kodiak Island, Alaska, *Ecoscience*, *1*(3), 255–267.

Piper, D. Z., and S. E. Calvert (2009), A marine biogeochemical perspective on black shale deposition, Earth Sci. *Rev.*, *95*, 63–96, doi:10.1016/j.earscirev.2009.03.001.

Piper, D. Z., and W. E. Dean (2002), Trace-element deposition in the Cariaco Basin, Venezuela Shelf, under sulfate-reducing conditions: A history of the local hydrography and global climate, 20 ka to the present, *U.S. Geol. Surv. Prof. Pap.*, *P1670*, 41 pp.

Powell, R. D., and B. F. Molnia (1989), Glacimarine sedimentary processes, facies and morphology of the south-southeast Alaska shelf and fjords, *Mar. Geol.*, *85*, 359–390, doi:10.1016/0025-3227(89)90160-6.

Price, N. M., B. A. Ahner, and F. M. M. Morel (1994), The equatorial Pacific Ocean: Grazer-controlled phytoplankton populations in an iron-limited ecosystem, *Limnol. Oceanogr.*, *39*(3), 520–534, doi:10.4319/lo.1994.39.3.0520.

Ragueneau, O., et al. (2000), A review of the Si cycle in the modem ocean: Recent progress and missing gaps in the application of biogenic opal as a paleoproductivity proxy, *Global Planet. Change*, *26*(4), 317–365, doi:10.1016/S0921-8181(00)00052-7.

Rasmussen, S. O., et al. (2006), A new Greenland ice core chronology for the last glacial termination, *J. Geophys. Res.*, *111*, D06102, doi:10.1029/2005JD006079.

Rea, D. K., and H. Snoeckx (1995), Sediment fluxes in the Gulf of Alaska: Paleoceanographic record from Site 887 on the Patton-Murray Seamount Platform, in *North Pacific Transect: Leg 145*, edited by D. K. Rea et al., *Proc. Ocean Drill. Program Sci. Results*, *145*, 247–256.

Rea, D. K., I. A. Basov, and L. A. Krissek (1995), Scientific results of drilling the North Pacific Transect, in *North Pacific Transect: Leg 145*,

edited by D. K. Rea et al., *Proc. Ocean Drill. Program Sci. Results*, *145*, 577–596.

Reger, R. D., A. G. Sturmann, E. E. Berg, and P. A. C. Burns (2008), A guide to the late Quaternary history of northern and western Kenai Peninsula, *Alaska Div. Geol. Geophys. Surv. Guidebook 8*, scale 1:63,360, 6 sheets, 112 pp., Alaska Div. of Geol. and Geophys. Surv., Ancorage.

Rind, D. (1998), Latitudinal temperature gradients and climate change, *J. Geophys. Res.*, *103*(D6), 5943–5971, doi:10.1029/97JD03649.

Rodionov, S. N., J. E. Overland, and N. A. Bond (2005), Spatial and temporal variability of the Aleutian climate, *Fish. Oceanogr.*, *14*, 3–21, doi:10.1111/j.1365-2419.2005.00363.x.

Rodionov, S. N., N. A. Bond, and J. E. Overland (2007), The Aleutian Low, storm tracks, and winter climate variability in the Bering Sea, *Deep Sea Res., Part II*, *54*, 2560–2577, doi:10.1016/j.dsr2.2007.08.002.

Rosenthal, Y., P. J. Lam, E. A. Boyle, and J. Thomson (1995), Authigenic cadmium enrichments in suboxic sediments: Precipitation and postdepositional mobility, *Earth Planet. Sci. Lett.*, *132*, 99–111, doi:10.1016/0012-821X(95)00056-I.

Royer, T. C. (2005), Hydrographic responses at a coastal site in the northern Gulf of Alaska to seasonal and interannual forcing, *Deep Sea Res., Part II*, *52*(1–2), 267–288, doi:10.1016/j.dsr2.2004.09.022.

Saito, M. A., J. W. Moffett, S. W. Chisholm, and J. B. Waterbury (2002), Cobalt limitation and uptake in *Prochlorocccus*, *Limnol. Oceanogr.*, *47*(6), 1629–1636, doi:10.4319/lo.2002.47.6.1629.

Sancetta, C. A., L. Heusser, L. Labeyrie, A. S. Naidu, and S. W. Robinson (1984), Wisconson-Holocene paleoenvironment of the Bering Sea: Evidence from diatoms, pollen, oxygen isotopes and clay minerals, *Mar. Geol.*, *62*, 55–68, doi:10.1016/0025-3227(84)90054-9.

Sarmiento, J. L., and N. Gruber (2006), *Ocean Biogeochemical Dynamics*, 503 pp., Princeton Univ. Press, Princeton, N. J.

Seki, O., M. Ikehara, K. Kawamura, T. Nakatsuka, K. Ohnishi, M. Wakatsuchi, H. Narita, and T. Sakamoto (2004), Reconstruction of paleoproductivity in the Sea of Okhotsk over the last 30 kyr, *Paleoceanography*, *19*, PA1016, doi:10.1029/2002PA000808.

Severmann, S., J. McManus, W. M. Berelson, and D. E. Hammond (2010), The continental shelf benthic iron flux and its isotope composition, *Geochim. Cosmochim. Acta*, *74*, 3984–4004, doi:10.1016/j.gca.2010.04.022.

Shiga, K., and I. Koizumi (1999), Latest Quaternary oceanographic changes in the Okhotsk Sea based on diatom records, *Mar. Micropaleontol.*, *38*, 91–117, doi:10.1016/S0377-8398(99)00041-9.

Springer, A. M., C. P. McRoy, and M. V. Flint (1996), The Bering Sea Green Belt: Shelf-edge processes and ecosystem production, *Fish. Oceanogr.*, *5*(3–4), 205–223, doi:10.1111/j.1365-2419.1996.tb00118.x.

Stabeno, P. J., J. D. Schumacher, R. F. Davis, and J. M. Napp (1998), Under-ice observations of water column temperature, salinity and spring phytoplankton dynamics: Eastern Bering Sea shelf, *J. Mar. Res.*, *56*(1), 239–255, doi:10.1357/002224098321836172.

Stabeno, P. J., N. A. Bond, N. B. Kachel, S. A. Salo, and J. D. Schumacher (2001), On the temporal variability of the physical environment over the south-eastern Bering Sea, *Fish. Oceanogr.*, *10*(1), 81–98, doi:10.1046/j.1365-2419.2001.00157.x.

Stabeno, P. J., N. A. Bond, A. J. Hermann, N. B. Kachel, C. W. Mordy, and J. E. Overland (2004), Meteorology and oceanography of the Northern Gulf of Alaska, *Cont. Shelf Res.*, *24*(7–8), 859–897, doi:10.1016/j.csr.2004.02.007.

Stabeno, P., J. Napp, C. Mordy, and T. Whitledge (2010), Factors influencing physical structure and lower trophic levels of the eastern Bering Sea shelf in 2005: Sea ice, tides and winds, *Prog. Oceanogr.*, *85*, 180–196, doi:10.1016/j.pocean.2010.02.010.

Steffensen, J. P., et al. (2008), High-resolution Greenland ice core data show abrupt climate change happens in few years, *Science*, *321*, 680–684, doi:10.1126/science.1157707.

Sundby, B., P. Martinez, and C. Gobeil (2004), Comparative geochemistry of cadmium, rhenium, uranium, and molybdenum in continental margin sediments, *Geochim. Cosmochim. Acta*, *68*(11), 2485–2493, doi:10.1016/j.gca.2003.08.011.

Talley, L. D. (1993), Distribution and formation of North Pacific Intermediate Water, *J. Phys. Oceanogr.*, *23*, 517–537, doi:10.1175/1520-0485(1993)023<0517:DAFONP>2.0.CO;2.

Thomson, R. E., and M. V. Krassovski (2010), Poleward reach of the California Undercurrent extension, *J. Geophys. Res.*, *115*, C09027, doi:10.1029/2010JC006280.

Thunell, R. C., D. M. Sigman, F. Muller-Karger, Y. Astor, and R. Varela (2004), Nitrogen isotope dynamics of the Cariaco Basin, Venezuela, *Global Biogeochem. Cycles*, *18*, GB3001, doi:10.1029/2003GB002185.

Trenberth, K. E., and J. W. Hurrell (1994), Decadal atmosphere–ocean variations in the Pacific, *Clim. Dyn.*, *9*(6), 303–319, doi:10.1007/BF00204745.

Tribovillard, N., T. J. Algeo, T. Lyons, and A. Riboulleau (2006), Trace metals as paleoredox and paleoproductivity proxies: An update, *Chem. Geol.*, *232*(1–2), 12–32, doi:10.1016/j.chemgeo.2006.02.012.

Van der Weijden, C. H. (2002), Pitfalls of normalization of marine geochemical data using a common divisor, *Mar. Geol.*, *184*(3–4), 167–187, doi:10.1016/S0025-3227(01)00297-3.

van Geen, A., Y. Zheng, J. M. Bernhard, K. G. Cannariato, J. Carriquiry, W. E. Dean, B. W. Eakins, J. D. Ortiz, and J. Pike (2003), On the preservation of laminated sediments along the western margin of North America, *Paleoceanography*, *18*(4), 1098, doi:10.1029/2003PA000911.

VanLaningham, S., N. G. Pisias, R. A. Duncan, and P. D. Clift (2009), Glacial-interglacial sediment transport to the Meiji Drift, northwest Pacific Ocean: Evidence for timing of Beringian outwashing, *Earth Planet. Sci. Lett.*, *277*, 64–72, doi:10.1016/j.epsl.2008.09.033.

Wagner, J. D. M., J. E. Cole, J. W. Beck, P. J. Patchett, G. M. Henderson, and H. R. Barnett (2010), Moisture variability in the southwestern United States linked to abrupt glacial climate change, *Nat. Geosci.*, *3*, 110–113, doi:10.1038/ngeo707.

Walinsky, S. E., F. G. Prahl, A. C. Mix, B. P. Finney, J. M. Jaeger, and G. P. Rosen (2009), Distribution and composition of organic matter in surface sediments of coastal southeast Alaska, *Cont. Shelf Res.*, *29*(13), 1565–1579, doi:10.1016/j.csr.2009.04.006.

Walsh, E. M., A. E. Ingalls, and R. G. Keil (2008), Sources and transport of terrestrial organic matter in Vancouver Island fjords and the Vancouver-Washington Margin: A multiproxy approach using dC13org, lignin phenols, and the ether lipid BIT index, *Limnol. Oceanogr.*, *53*(3), 1054–1063, doi:10.4319/lo.2008.53.3.1054.

Weber, S. L., F. Niessen, G. Kuhn, and M. Wiedicke (1997), Calibration and application of marine sedimentary physical properties using a multisensor core logger, *Mar. Geol.*, *136*, 151–172, doi:10.1016/S0025-3227(96)00071-0.

Weingartner, T. J., et al. (2002), The Northeast Pacific GLOBEC Program: Coastal Gulf of Alaska, *Oceanography*, *15*(2), 48–63.

Whitney, F. A., D. W. Crawford, and T. Yoshimura (2005), The uptake and export of silicon and nitrogen in HNLC waters of the NE Pacific Ocean, *Deep Sea Res., Part II*, *52*(7–8), 1055–1067, doi:10.1016/j.dsr2.2005.02.006.

Wiles, G. C., D. J. Barclay, and P. E. Calkin (1999), Tree-ring-dated 'Little ice age' histories of maritime glaciers from western Prince William Sound, Alaska, *Holocene*, *9*(2), 163–173, doi:10.1191/095968399671927145.

Wong, C. S., R. J. Matear, H. J. Freeland, F. A. Whitney, and A. S. Bychkov (1998), WOCE line P1W in the Sea of Okhotsk: 2. CFCs and the formation rate of intermediate water, *J. Geophys. Res.*, *103*, 15,625–15,642, doi:10.1029/98JC01008.

Wu, J. P., S. E. Calvert, and C. S. Wong (1997), Nitrogen isotope variations in the subarctic northeast Pacific: Relationships to nitrate utilization and trophic structure, *Deep Sea Res., Part I*, *44*(2), 287–314, doi:10.1016/S0967-0637(96)00099-4.

You, Y., N. Suginohara, M. Fukasawa, I. Yasuda, I. Kaneko, H. Yoritaka, and M. Kawamiya (2000), Roles of the Okhotsk Sea and Gulf of Alaska in forming the North Pacific Intermediate Water, *J. Geophys. Res.*, *105*, 3253–3280, doi:10.1029/1999JC900304.

Zahn, R., T. F. Pedersen, B. D. Bornhold, and A. C. Mix (1991), Water mass conversion in the glacial subarctic Pacific (54°N, 148°W): Physical constraints and the benthic-planktonics stable isotope record, *Paleoceanography*, *6*, 543–560, doi:10.1029/91PA01327.

J. A. Addison, U.S. Geological Survey, 345 Middlefield Rd., MS 910, Menlo Park, CA 94025, USA. (jaddison@usgs.gov)

M. H. Davies, A. C. Mix, and J. S. Stoner, College of Ocean and Atmospheric Sciences, Oregon State University, 104 COAS Administration Bldg., Corvallis, OR 97331-8563, USA. (mdavies@coas.oregonstate.edu; mix@coas.oregonstate.edu; jstoner@coas.oregonstate.edu)

W. E. Dean, U.S. Geological Survey, MS 980, Box 25045, Denver Federal Center, Denver, CO 80225, USA. (dean@usgs.gov)

B. P. Finney, Department of Biological Sciences, Idaho State University, Pocatello, ID 83209-8007, USA. (finney@isu.edu)

J. M. Jaeger, Department of Geological Sciences, University of Florida, 241 Williamson Hall, PO Box 112120, Gainesville, FL 32611, USA. (jmjaeger@ufl.edu)